Refined Structure of an Intact IgG2a Monoclonal Antibody[†,‡]

Lisa J. Harris,[§] Steven B. Larson,[§] Karl W. Hasel,[||] and Alexander McPherson*[,§]

Department of Biochemistry, University of California, Riverside, California 92521, and QED BioScience, 11021 Via Frontera, San Diego, California 92127

Received October 7, 1996; Revised Manuscript Received November 27, 1996[⊗]

ABSTRACT: The structure of an intact, anti-canine lymphoma monoclonal antibody (Mab231)[1] was determined by molecular replacement and refined in a triclinic cell to an *R*-value of 20.9%, using synchrotron diffraction data from 2.8 to 20 Å resolution. All segments of the antibody, including the hinge region and carbohydrate component, are visible in electron density maps. There is no overall symmetry to the antibody, as the Fc is disposed in an entirely oblique manner with respect to the Fabs. The C_H2 and C_H3 domains do, however, possess a nearly exact, local 2-fold relationship. The Fab segments are related by a second, independent, local dyad axis, exact only with respect to constant domains. Variable domains exhibit no symmetry relationship as a consequence of the 16° difference in Fab elbow angles. Variable domain pair associations V_L:V_H for the Fabs are virtually the same, and corresponding CDRs of the two Fabs also are nearly identical in structure. CDR-H3 displays the greatest difference. Hypervariable loops of both Fabs are involved in contacts with symmetry-related Fc segments at the C_H2-C_H3 switch junction, suggesting a "complex" structure. The hinge segment connecting Fabs with the Fc is quite extended and exhibits thermal factors indicative of a high degree of mobility. It consists of a well-defined upper hinge that partially maintains dyad symmetry and a fairly rigid core bounded above and below by fluid polypeptides that provide segmental flexibility. This structure represents the first visualization by X-ray analysis of a murine Fc segment, and its C_H2 domains exhibit substantial rigid body conformational changes with respect to the human Fc used as an initial molecular replacement model. The oligosaccharides were found by difference Fourier syntheses to be very similiar to those of the free human Fc fragment, although differences are present in the terminal residues. The detailed structure of the IgG presented here, and the distribution of effector binding sites, appears consistent with effector activation mechanisms involving translocation and/or aggregation of the Fc following antigen binding by the Fabs.

Antibodies are flexible glycoproteins that can assume a wide range of conformations as a consequence of intrinsic domain mobility or segmental flexibility (Wrigley *et al.*, 1983; Roux, 1984; Wade *et al.*, 1989; Schneider *et al.*, 1988; Dangl *et al.*, 1988; Huber *et al.*, 1976; Amzel & Poljak, 1979). This mobility contributes to their dual function of recognizing and subsequently eliminating foreign bodies, such as viruses or bacteria. Antigen recognition and binding occurs through Fab segments, while the Fc portion of the molecule is principally responsible for effector functions. Intact IgG is composed of two identical light chains (L) and two identical heavy chains (H) which form two Fabs and one Fc segment for a total of 12 domains which associate in pairs (V_L:V_H, C_L:C_H1, C_H2:C_H2, and C_H3:C_H3). Six hypervariable loops (L1, L2, L3, H1, H2, H3) make up the antigen binding site on the variable domain pair V_L:V_H of each Fab [for review, see Davies and Chacko (1993)].

A large number of Fab fragments have been investigated, and the three-dimensional structure of their four β-barrel domains (V_L, V_H, C_L, C_H1) is well established [for reviews, see Alzari *et al.* (1988), Colman (1988), Davies *et al.* (1990), Mian *et al.* (1991), Davies and Chacko (1993), Edmundson *et al.* (1993), Sheriff (1993a), Wilson and Stanfield (1994), and Padlan (1994)]. The Fc fragment of a human antibody has also been solved; thus the structure of this portion of the molecule and its four β-barrel domains (C_H2, C_H2, C_H3, C_H3) is likewise known (Deisenhofer, 1981).

Other intact antibody structures have been studied by X-ray crystallography (Silverton *et al.*, 1977; Guddat *et al.*, 1993; Marquart *et al.*, 1980). In two myeloma proteins, the flexible hinge regions connecting Fab and Fc segments were deleted (Silverton *et al.*, 1977; Guddat *et al.*, 1993). The molecules were structurally restrained and, perhaps for this reason, appeared as compact T-shapes, the angle between Fabs close to 180°. A third antibody, Kol, had an intact hinge, but the Fc was so disordered that it was not possible to orient it with respect to the Fabs (Marquart *et al.*, 1980). The two Fabs and a portion of the hinge (upper and core) were, however, visualized. The angle between the Fabs was 120° so that the Kol antibody assumed a distorted Y-shape. For all three antibody structures a crystallographic dyad related the visible halves of the molecules. The anti-canine lymphoma antibody (CL/Mab231), described here, contains an intact hinge, and both the Fabs as well as the Fc are ordered (Harris *et al.*, 1992).[1]

Monoclonal antibody 231 (murine IgG2aκ) binds specifically to malignant canine lymphocytes and mediates antibody-dependent cellular cytotoxicity (ADCC) as well as comple-

[†] This research was supported by grants from NASA, NSF, and QED BioScience.

[‡] Atomic coordinates of the IgG2a intact antibody Mab231 are deposited in the Brookhaven Protein Data Bank with access code 1IGT.

[§] University of California.

[||] QED BioScience.

[⊗] Abstract published in *Advance ACS Abstracts,* February 1, 1997.

[1] The residue numbering convention for the entire paper is that of Kabat *et al.* (1991). Atomic coordinates are deposited with the Brookhaven Protein Data Bank using this same numbering system.

S0006-2960(96)02514-7 CCC: $14.00

ment-dependent cytotoxicity (CDC) (Rosales *et al*., 1988). Chemotherapy in combination with adjuvant Mab231 treatment prolongs cancer remission and survival times of afflicted dogs (Jeglum, 1989). For therapeutic use, CL/Mab231 is commercially available from Synbiotics Inc., San Diego, CA. The canine lymphoma antibody has additionally been shown to internalize following antigen binding; consequently, antitumor antibiotics, conjugated to Mab231 for site-specific delivery, are potential cancer therapeutics. Canine lymphoma is an animal model for human non-Hodgkin's lymphoma and could serve as an intermediary model for applications of immunoconjugate therapy in human lymphoma patients.

MATERIALS AND METHODS

Crystallization. Mab231 was crystallized at 18 °C from 4% poly(ethylene glycol) (PEG) 3350 at pH 7.8−8.2 (Larson *et al*., 1991; Harris *et al*., 1995). Crystals were triclinic with $a = 65.82$ Å, $b = 76.77$ Å, $c = 100.64$ Å, $\alpha = 88.05°$, $\beta = 92.35°$, and $\gamma = 97.23°$ ($Z = 1$). The solvent content of the crystals was 63%.

Carbohydrate Analysis. Carbohydrate composition analysis (Protein and Carbohydrate Structure Facility, Ann Arbor, MI) of the Mab231 protein used for crystallization indicated the presence of fucose, *N*-acetylglucosamine, mannose, and galactose, sugars typical for N-linked chains. Two Asn-X-Ser/Thr sequences are located on Mab231, one on each C_H2 domain. Absence of *N*-acetylgalactosamine revealed that O-linked sugars are not present.

X-ray Diffraction. Diffraction intensities were initially collected on a San Diego Multiwire Systems (Xuong-Hamlin) area detector system with two detector panels mounted on a two-theta table (Xuong *et al*., 1985). The X-ray source was a Rigaku RU-200 rotating anode operated at 45 kV and 175 mA and fitted with a Supper Co. graphite crystal monochromator to produce Cu Kα radiation. The frame size was 0.12° and counting times were 60−120 s. Crystals ranging in size up to 1.5 mm in the longest dimension were mounted in quartz X-ray capillaries by conventional means for data collection at 18 °C. The multiwire data were processed using the programs of Howard and Nielsen (Hamlin *et al*., 1981). More than 200 000 observations from 13 crystals were merged to 47 595 unique reflections with R_{sym} of 10% at 2.8 Å. These were subsequently cut at $F > 4.0\sigma$ to give a reduced data set at 2.8−20 Å of 32 838 unique reflections (68% complete).

Intensities were later collected at the Stanford Synchrotron Radiation Laboratory in order to obtain additional high-resolution data for structure refinement. A MAR Research imaging plate with diameter 180 mm and a crystal-to-detector distance of 150 mm was used. Radiation was from a 1 mrad side station on an eight pole EM wiggler (wavelength 1.08 Å). The beam was focused to 0.2 × 0.2 mm. The oscillation scan was 1.0° or 2.0°, and the exposure per image ranged from 10 s (in time mode) to 2000−3000 counts/kHz (in dose mode). Data were processed with the program MOSFLM (Leslie *et al*., 1992). A total of 180 376 observations from 13 crystals were merged to give 47 722 unique reflections with an R_{sym} of 13% at 2.8 Å. Reflections were then cut at $F > 4.0\sigma$ to give a reduced data set from 2.8 to 20 Å of 38 299 unique reflections (80% complete).

The multiwire and synchrotron data sets with $F > 4.0\sigma$ were combined to yield a reduced, working data set of 41 371 unique reflections (86% complete) at 2.8−20.0 Å with an R_{merge} of 6.7%.

Table 1: Structure Solution[a]

self-rotation	ϕ (deg)	ψ (deg)	κ (deg)	rms	resolution (Å)
primary local dyad	60	50	180	3.54	4−8
secondary local dyad	0	60	180	3.17	5−10

Fc cross rotation	α (deg)	β (deg)	γ (deg)	rms	rms (NP)	S/N
entire Fc	125	137.5	10	6.03		
dyad related peak	305	37.5	5	5.54	3.85	1.57
C_H3:C_H3	same peaks as Fc			5.66		
				5.64	4.13	1.37
C_H2:C_H2	same peaks as Fc			3.41		0.92
				3.14		0.85

Fab1 cross rotation	α (deg)	β (deg)	γ (deg)	rms	rms (NP)	S/N
C_L:C_H1 HYHEL-5	80	135	180	6.42	4.67	1.37
V_L:V_H 1McPC603	70	130	180	4.35	4.17	1.04
intact Fab1 constructed from above CON and VAR results; elbow 160°	80	135	180	7.98	4.32	1.85

Fab2 cross rotation	α (deg)	β (deg)	γ (deg)	rms	rms (NP)	S/N
Fab2 constucted from Fab1 but with elbow 140°	315	77.5	300	6.27	4.99	1.26

translation	translation vector	CC
Fab1 against fixed Fc	(−0.01 -0.30 0.31)	0.224
Fab2 against fixed Fc	(−0.16 -0.16 0.17)	0.209

[a] NP, next peak; S/N, signal to noise (the ratio of the two peak heights); CC, correlation coefficient; self-rotation expressed in polar angles; cross-rotation expressed in Euler angles; translation vector expressed in fractional coordinates; MERLOT (Fitzgerald, 1988) cross-rotation searches and X-PLOR (Brünger, 1991) translation searches are stated for 4−8 Å resolution. For the Fc orientation results, the pseudodyad relating the two peaks corresponded to the dyad indicated by the primary self-rotation solution. The secondary self-rotation dyad related the two Fabs with respect to their constant domains only. The next peak in both the C_L:C_H1 and the V_L:V_H search was determined in retrospect to be the correct orientation for Fab2's independent domain pair (second peak in both cases).

Computational Techniques. Two molecular replacement systems were employed, MERLOT (Fitzgerald, 1988) and X-PLOR (Brünger, 1991). Refinement was carried out with X-PLOR (Brünger, 1991). Graphics were performed with the programs FRODO (Jones, 1978) and "O" (Jones & Kjeldgaard, 1994). Least squares superposition of equivalent Cαs was implemented with the Lsq options in "O" and the Fit option in X-PLOR. GRASP (Nicholls *et al*., 1991) was used for an electrostatic analysis of the antibody surface. Buried surface areas were calculated with MS (Connolly, 1983), and hypervariable loop packing interactions with CONTACTSYM (Sheriff, 1993b). Stereochemical quality of the structure was assessed using PROCHECK (Laskowski *et al*., 1993). Images were generated with the program SETOR (Evans, 1993), except Figure 8A which was made with "O". The computers used were a VAX network, Evans & Sutherland PS 390, Silicon Graphics Iris 340 VGX, and Cray C90.

Structure Determination. Molecular Replacement was utilized to solve the antibody structure as summarized in Table 1. The triclinic unit cell did not constrain the molecule conformationally or impose any symmetry on the IgG. The

lack of crystal symmetry did not, however, rule out global symmetry as seen for other intact antibodies (Silverton *et al*., 1977; Guddat *et al*., 1993; Marquart *et al*., 1980), nor did it preclude local symmetry.

(A) Self-Rotation Search. Using MERLOT, self-rotation functions were calculated for 20 different resolution ranges (with and without origin removal) to determine the presence, or lack of, symmetry within the intact molecule (Table 1). A dyad axis was indicated and was consistent among the functions computed but was not as impressive ($\phi = 60°$, $\psi = 50°$, $\kappa = 180°$; rms 3.54, top peak at 4−8 Å), as would be expected from an antibody exhibiting global dyad symmetry. A secondary peak ($\phi = 0°$, $\psi = 60°$, $\kappa = 180°$; rms 3.17, top peak at 5−10 Å) competed with the primary solution and persisted throughout the analysis. Both dyad solutions were weak and therefore considered possible local dyads. The angle between the two putative dyads was 120°.

(B) Cross-Rotation Search. Molecular probe coordinates for seven Fab fragments (Satow *et al*., 1986; Sheriff *et al*., 1987; Padlan *et al*., 1989; Suh *et al*., 1986; Lascombe *et al*., 1989; Poljak *et al*., 1974; Marquart *et al*., 1980) and an Fc fragment (Deisenhofer, 1981) were from the Brookhaven Protein Data Bank (Bernstein *et al*., 1977), PDB entry codes 1MCP, 2HFL, 3HFM, 1FBJ, 1F19, 3FAB, 2IG2, and 1FC1. The fast rotation of Crowther and Blow (Crowther, 1972) implemented in MERLOT was used. Cross rotation searches were performed with probes representing one-third of the asymmetric unit (one-third of the antibody) and with probes comprising only one-sixth of the asymmetric unit. Searches were performed with data for which $F > 4.0\sigma$ over three resolution ranges: 3.5−7.0 Å, 4.0−8.0 Å, and 5.0−10.0 Å with Patterson cutoff radii of 20.9, 23.9, and 29.9 Å, respectively. Probe structure factors were calculated in an artificial unit cell 150 Å × 150 Å × 150 Å. Searches were restricted to the asymmetric unit of rotation function space, $\alpha = 0° -360°$, $\beta = 0°-180°$, and $\gamma = 0°-360°$; increments of α and γ were 5° and of β 2.5°. Functions were computed both with and without origin removal.

Prior to cross rotation calculations, a reference orientation was chosen so that the major axis of the Fc probe was placed along crystallographic *x*, and Fabs from Kol were placed in the triclinic *xz* plane to form a model antibody patterned after Marquart *et al*. (1980) with center of mass at the origin. The constant domains (CON) of all Fab structures from the PDB were superimposed onto the CON domains of a Kol Fab to establish a common reference orientation for the C_L:C_H1 probes as well as for entire Fab models. Variable domains (VAR) of the structures were then superimposed to provide the reference orientation for V_L:V_H models.

Searches using the human Fc fragment (Deisenhofer, 1981) lacking carbohydrate as a probe structure revealed the orientation of the Fc segment of Mab231 (Table 1). Two pronounced peaks well above the next highest peak (S/N = 1.57) were consistently present and related by a dyad axis. The dyad related the two heavy chains of the Fc and corresponded to the 2-fold axis indicated by the primary solution of the self-rotation function. Separate searches were also carried out with only C_H3 domains and then C_H2 domains. The C_H3:C_H3 search revealed the same outstanding dyad-related peaks as did that with entire Fc, demonstrating that unambiguous solutions could emerge using probes representing only one-sixth of the asymmetric unit. A search with C_H2:C_H2 also revealed the same solution as for the entire Fc segment, but less clearly. Because of the triclinic space group, the center of mass of the entire antibody could be placed at an arbitrary position in the unit cell (0, 0, 0 chosen) and thereby establish an origin. The Fc segment was oriented and positioned in the P1 cell and became the cornerstone for the remainder of the structure analysis.

Fabs are flexible at their switch peptides, connecting VAR to CON domains, and their "elbow angle" is defined as the angle between the pseudo-2-fold axes relating C_H1 to C_L and V_H to V_L, respectively. Elbow angles have been observed from 127° to 227° [see review by Wilson and Stanfield (1994)]. No basis existed for assuming Fab elbow angles to be the same in this intact antibody.

To obviate the problem of unknown elbow angle, and to obtain the best models for Mab231 domains, the CON and VAR domains of Fabs from the PDB were used separately as probes. One exceptionally strong peak resulted from the search with C_L:C_H1 of Fab HyHEL-5 (Sheriff *et al*., 1987) and was consistent throughout the various resolution ranges (Table 1). This orientation for the CON domains of Fab1 of the antibody (termed Fab1 because its orientation was first determined) was consistent with joining to the Fc. No orientation for Fab2 CON domains was realized. An optimal solution appeared using V_L:V_H of Fab McPC603 (Satow *et al*., 1986), including hypervariable regions, but again no orientation for a second Fab could be discerned. The solution allowed McPC603 VAR domains to be joined to the correctly oriented CON domains in a manner consistent with known Fab structure. A composite Fab1 probe, made according to these orientations and domain models, yielded an outstanding rotation peak with rms 7.98 and S/N = 1.85. Again, no solution for Fab2 was apparent, and Fab2 was assumed likely to have a different elbow angle.

With constant domains of Fab HyHEL-5 and variable domains of Fab McPC603, the model Fab1 was modified in its elbow (using X-PLOR elbow.inp) to construct multiple probes having elbow angles covering the range of 120°−180°, in increments of 5°. MERLOT rotation function searches using each model clearly indicated the correct orientation for Fab2 (Table 1 and Figure 1). The orientation for Fab2 revealed in these searches was also consistent with joining to the Fc. In Figure 1, the elbow angle of Fab1 was arbitrarily set to zero; thus the best solution for Fab2's orientation was the probe having elbow angle −20°. The optimum models for Fab1 and Fab2 had elbow angles of 160° and 140°, respectively.

(C) Translation Search. Because the antibody model was assembled from fragments, relative distances between the two Fabs and Fc had to be determined. This was accomplished using the translation function implemented in X-PLOR (Table 1). Since it involved three segments, a redundancy existed. Two solutions would define the system, but all solutions had to be self-consistent. Searches were computed over the entire unit cell in 0.01 increments. The top peak in each case was the correct solution, and all results were self-consistent.

(D) Crystal Packing. The antibody molecule was assembled according to independent, but internally consistent, molecular replacement results. Confirmation of the structure emerged from inspection of crystal packing which revealed an intricate complimentarity of surfaces. Only minor contact problems involving hypervariable loops were observed. In

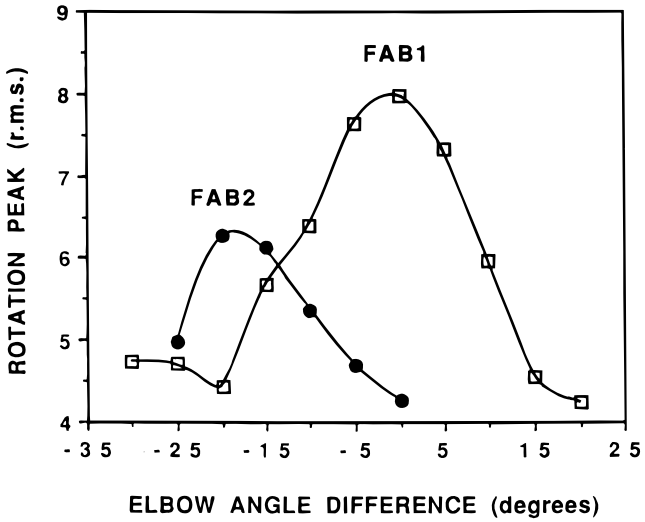

FIGURE 1: Orientation solutions for Fab1 and Fab2 as a function of elbow angle, based on results from Crowther's fast cross-rotation function (Crowther, 1972) using 4−8 Å resolution. The curve for Fab1 corresponds to the rotation peak solution $\alpha = 80°$, $\beta = 135°$, and $\gamma = 180°$ (□). The curve for Fab2 corresponds to the rotation peak $\alpha = 315°$, $\beta = 77.5°$, and $\gamma = 300°$ (●). No points are indicated for either of these two solutions if rms < 4.0. The optimum search probe for Fab1 had an elbow angle of 160° and for Fab2 an angle of 140°. When a probe with an intermediary elbow angle was used (145−150°), then the top two peaks of the function were the orientations for both Fab1 and Fab2, respectively, but this probe was not the optimum model for either.

addition, lattice contacts served to immobilize all segments of the molecule, thereby imposing order throughout the crystal.

Refinement. Refinement was carried out with the program X-PLOR, Version 3.1 (Table 2). A bulk solvent mask was employed upon inclusion of low-resolution data to 20 Å. The model was fitted to both $2F_o - F_c$ and $F_o - F_c$ electron density maps using FRODO and "O". Rebuilding was predominantly with $F_o - F_c$ omit maps which were calculated after removing 50-residue segments of the model (∼4% of the asymmetric unit) followed by 40 cycles of Powell minimization. Grouped temperature factor refinement was performed with the backbone and side chains of each amino acid as groups; each sugar residue was treated as a single group. Noncrystallographic symmetry restraints were used for equivalent constant domains during simulated annealing and Powell minimization (see below for details).

The structure was initially refined using multiwire data (Harris *et al.*, 1992). Rigid body refinement of the Fc and Fabs yielded an *R*-value of 43.4% and a correlation coefficient (CC) of 0.38 at 3.5−12.0 Å, and six domain pairs yielded an *R* of 41.3% and CC of 0.45. Twelve β-barrels refined independently as rigid groups produced an *R*-value of 38.6% and CC of 0.53. When the sequence for the intact antibody became available, corresponding domains of Mab231 were found to be 67% identical to V_L and 64% to V_H of mouse IgAκ McPC603; 100% to C_L and 85% to C_H1 of mouse IgG1κ HyHEL-5; and 65% to the human IgG1 Fc fragment. Minor problems with crystal packing had involved CDRs of Fab McPC603, but problematic residues corresponded to deletions in Mab231. Twenty-three residues in each heavy chain, corresponding to the hinge regions, were inserted to connect Fab segments with the Fc segment according to geometric constraints. Artificial coordinates were made for these regions, based on recommended

Table 2: Data and Refinement Statistics

space group	*P*1
unit cell	$a = 65.82$ Å, $b = 76.77$ Å, $c = 100.64$ Å, $\alpha = 88.05°$, $\beta = 92.35°$, $\gamma = 97.23°$
data completeness	41 371 unique reflections ($F > 4\sigma$) from 2.8 to 20 Å

resolution range (Å)	% completeness	% accumulative ($F > 4\sigma$)
3.52−20.00	97.7	97.7
3.32−3.52	89.3	96.3
3.15−3.32	83.4	94.5
3.02−3.15	74.9	92.0
2.90−3.02	67.5	89.3
2.80−2.90	59.0	86.2

refinement statistics[a]	
resolution limits	2.8−20 Å
R-value	20.9%
correlation coefficient	0.83
no. of unique reflections in working set ($F > 4\sigma$)	37 222
free *R*-value	29.7%
free correlation coefficient	0.70
no. of unique reflections in test set ($F > 4\sigma$)	4 149
no. of molecules in asymmetric unit	1
no. of total non-hydrogen atoms in final model	10 416
no. of solvent molecules	none included
average protein *B*-value	51 Å^2
average carbohydrate *B*-value for chain 1 and 2	70 and 143 Å^2
rmsd in protein bond lengths	0.009 Å
rmsd in protein bond angles	1.6°
rmsd in carbohydrate bond lengths	0.008 Å
rmsd in carbohydrate bond angles	1.4°

[a] Noncrystallographic symmetry restraints were used for equivalent constant domains of the antibody during X-PLOR refinement (Brünger, 1991). *R*-value $= \sum_{hkl}(||F_{o_{hkl}}| - |F_{c_{hkl}}||)/\sum_{hkl}|F_{o_{hkl}}|$, where $|F_{o_{hkl}}|$ and $|F_{c_{hkl}}|$ are the observed and calculated structure factor amplitudes.

procedures for generating a structure with missing residues (Brünger, 1991), and occupancies set to zero for ensuing refinement. At 3.5−8.0 Å a single cycle of X-PLOR refinement, using the correct amino acid sequence, yielded a model with an *R*-value of 18.8% and CC of 0.88. An overall *B*-factor of 15 Å^2 was maintained.

Final refinement was conducted using combined multiwire and synchrotron data from 2.8 to 20 Å (Table 2). The initial pass with the higher resolution data yielded an *R*-value of 24.4% and CC 0.77. After sequential cycles of manual model rebuilding with "O", simulated annealing, Powell minimization, and grouped *B*-factor refinement, the *R*-value declined to 22.1% and the free *R*-value to 30.4%. At each stage, the occupancy of only clearly defined hinge and carbohydrate residues were set to one, while the rest were represented as artificial coordinates with occupancies of zero. The model, at this point, contained most of the carbohydrate component and about one-third of the hinge residues which were absent in the original model. Noncrystallographic symmetry (NCS) restraints were then employed for corresponding constant domains (Kleywegt & Jones, 1995; Kleywegt & Jones, 1996). Parallel slow-cooling cycles were run with various stringencies for NCS to determine an optimum refinement protocol. A noncrystallographic symmetry operator was specified separately for each individual domain (C_L, C_H1, C_H2, C_H3) to account for possible differences in domain dispositions. Only backbone atoms of residues not involved in packing contacts were restrained. An NCS force constant of 200 for backbone atoms was used, and side chains were not restrained. This protocol produced

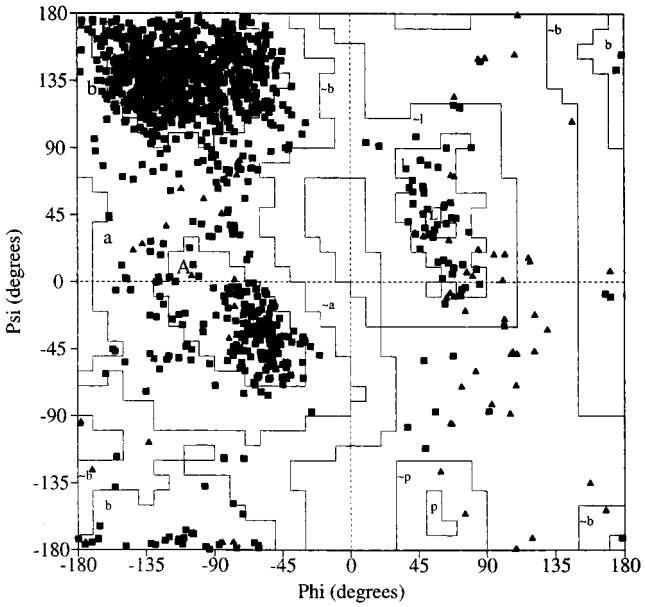

FIGURE 2: Ramachandran plot of the main chain stereochemical quality for the intact Mab231 structure, calculated with the program Procheck (Laskowski *et al*., 1993). The total number of protein residues is 1316, of which 1134 are non-glycine and non-proline: 896 non-glycine/non-proline amino acids are in the most favored regions (79.0%); 215 are in additional allowed regions (19.0%); 15 are in generously allowed regions (1.3%); and 8 are in disallowed regions (0.7%). Glycines are indicated by triangles.

an *R*-value and free *R*-value that were similar as before (22.5% and 30.3%); however, main chain stereochemical parameters for 38 residues improved significantly. Other NCS refinement protocols resulted in either higher free *R*-values or main chain parameters of lower quality.

Alternating cycles of individual *B*-factor and positional refinement were performed at the end of the process. NCS restraints were not applied to individual temperature factors, because domains of Mab231 had notably different average *B*-factors (see below). While one could expect the *R*-value to decrease as a consequence of more parameters, the model was judged to be improved as density for additional hinge residues became visible and the free *R*-value declined 0.6%.

The *R*-value for the antibody structure converged to 20.9%, the free *R*-value to 29.7%, a CC of 0.83, and a free CC of 0.70. The final model contains all 18 sugar residues and the entire hinge region, except for six side chains of the lower hinge which have occupancies of zero. No water molecules are included. rms deviations from ideal geometry are 0.009 Å for bonds and 1.6° for angles. According to PROCHECK, eight of ten of the stereochemical parameters are "BETTER"; the remaining two are categorized as "Better" (Ramachandran plot and Zeta angle standard deviation) (Figure 2). The average temperature factor for all protein atoms is 51 Å^2; oligosaccharide chain 1 and chain 2 are 70 Å^2 and 143 Å^2, respectively. Average *B*-factors vary significantly by IgG domain depending on crystal packing. Domain *B*-factor averages, for backbone atoms, range from minimum values of 24 Å^2 for V_H of Fab2 and 26 Å^2 for C_H2 of heavy chain 1 to the maximum value of 100 Å^2 for C_H2 of heavy chain 2. Most domains, however, average about 40 Å^2.

RESULTS AND DISCUSSION

Domain Dispositions. The triclinic symmetry of the crystal unit cell places no constraints on the conformation

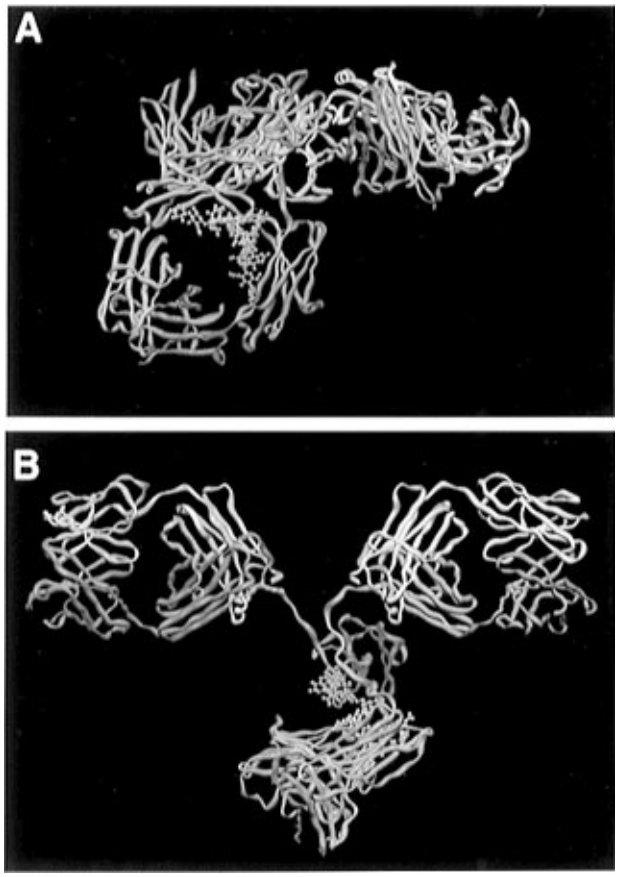

FIGURE 3: (A) Monoclonal antibody 231 viewed perpendicularly to the nearly exact 2-fold axis relating heavy chains of the Fc segment. Cα superposition of the Fc heavy chains as rigid units yields an rms deviation of 0.90 Å with a rotation of 179.3°. This dyad corresponds to that indicated by the primary solution of the self-rotation function. Light chains are in gold and light blue, while heavy chains are in orange and medium blue. Carbohydrate components, shown in ball and stick, are N-linked through Asn residues to the C_H2 domains of the Fc fragment. The oligosaccharides are consistent with the pseudodyad relating the C_H2 domain pair. (B) Intact antibody viewed perpendicularly to the nearly exact dyad axis relating constant domains of the Fabs. Cα superposition of Fab2 C_L:C_H1 onto Fab1 C_L:C_H1 yields an rms deviation of 0.51 Å with a rotation of 179.4°. This dyad is that indicated by the secondary solution of the self-rotation function. The variable domains are not related by this 2-fold axis as a consequence of different elbow angles for the Fabs. Fab1 has an elbow angle of 159°, in contrast to 143° for Fab2. Also seen in this view is the failure of the Fc dyad axis to intersect the 2-fold axis relating the Fab constant domains.

of the antibody, and indeed the molecule exhibits no overall symmetry. Local dyad relationships are, however, present within, or between, individual segments (Figure 3 and Table 3). These include a nearly exact dyad relating the Fc heavy chains and a nearly exact 2-fold axis between the constant domain pairs (C_L:C_H1) of the Fabs. Variable domain pairs (V_L:V_H) violate this restraint only as a consequence of differing Fab elbow angles, 159° for Fab1 and 143° for Fab2. The long axes of the two Fabs are close to collinear, so that a single axis runs approximately through both segments. The greatest dimension of the molecule is 161 Å, from Fab1 hypervariable loop H2 (Gly55 Cα) to the corresponding Fab2 H2 (Gly55 Cα). The orientation of the Fc, with respect to the Fabs, is oblique, with hinge angles between Fab1 and Fc of about 65° and between Fab2 and Fc of 115°. The dyad axis of the Fc does not intersect that relating the Fab constant domains or the approximate long axis of the Fabs.

Table 3: Local Pseudo-2-fold Symmetry[a]

dyad	rotation (deg)	rmsd (Å)
Fab1 C_L:C_H1 and Fab2 C_L:C_H1	179.4	0.51
Fc heavy chains	179.3	0.90

	C_H2:C_H2 symmetry rotation (deg)	C_H3:C_H3 symmetry rotation (deg)
Fc	177.8	178.8

	V_L:V_H symmetry		C_L:C_H1 symmetry		
	rotation (deg)	translat (Å)	rotation (deg)	translat (Å)	elbow (deg)
Fab1	172.2	0.1	167.4	−1.7	159
Fab2	173.2	−0.1	167.3	−1.8	143

[a] Structually equivalent Cαs were superimposed to determine the rotation angles. Superposition was implemented with both the Lsq options in "O" (Jones & Kjeldgaard, 1994) and the Fit option in X-PLOR (Brünger, 1991).

The two local dyads are not coupled, thereby permitting nearly independent movement of the Fc and Fabs.

The local 2-fold axis relating the Fc heavy chains was anticipated and not found exceptional in light of previous X-ray analyses (Deisenhofer, 1981; Silverton *et al*., 1977; Guddat *et al*., 1993), but it is not apparent why such a relationship persists between the constant domain pairs of the Fabs. No crystallographic constraint imposes the dyad, nor does there appear to be any clear stereochemical explanation.

The structure of a second intact monoclonal antibody, specific for the drug phenobarbital, has also been solved by X-ray crystallography in our laboratory (paper in preparation). This murine IgG1 exhibits the same essential features as were observed in the anti-lymphoma IgG2a molecule, an overall asymmetry with two independent local dyads obliquely disposed. Some details, however, such as hinge and elbow angles, and the angle between Fab segments, are quite different.

Noncrystallographic symmetry restraints were employed during the course of refinement for equivalent constant domains of the CL/Mab231 immunoglobulin (C_L, C_H1, C_H2, C_H3), but residues involved in packing contacts were not restrained. Noncrystallographic symmetry, furthermore, was not used in refinement of the variable domains; thus, any similarities between corresponding variable portions of the molecule are unbiased.

Electron density maps for the molecule were, in general, of good quality and side chains could be unambiguously positioned (Figure 4). Hypervariable regions were stabilized in the crystal through packing interactions and were clearly visible. The electron density presented in Figure 4A along with the corresponding structure for hypervariable loop H3 of Fab2 is representative of the density for all 12 of the hypervariable loops. Of the 12 β-barrel domains, the C_H2 domain of heavy chain 2 experiences the fewest crystal packing interactions and the most exposure to solvent. This was the only domain where interrupted density presented noteworthy ambiguities. The problematic regions were confined primarily to the upper half of the domain most distant from the C_H2-C_H3 junction, consistent with observed high temperature factors (Figure 5). In the human Fc fragment (Deisenhofer, 1981), the Fc fragment/fragment B of protein A complex (Deisenhofer, 1981), and the Fc fragment/rat neonatal Fc receptor complex (Burmeister *et al*., 1994), the upper portions of the C_H2 domains were also poorly ordered. For the other 11 Mab231 domains, electron density displayed minor discontinuities in only a few exterior loops.

Variable and Hypervariable Regions. The triclinic crystal presented an opportunity to compare an intact antibody's two Fab segments exposed to different chemical environments. As noted above, elbow angles relating Fab constant and variable domains are different, but V_L and V_H associate nearly identically for both Fabs (Figure 6 and Table 3). In Figure 6, the variable domain pair V_L:V_H of Fab2 is shown superimposed onto the respective domain pair of Fab1. The rms deviation is 0.59 Å using all Cαs. Rearrangements of variable domains have been observed where both free and antigen complexed Fabs were determined crystallographically (Wilson *et al*., 1991; Stanfield *et al*., 1993; Edmundson *et al*., 1994; Ban *et al*., 1995). The majority of V_L-V_H rearrangements seen, thus far, fall within the range of 2°−6° [see review by Wilson and Stanfield (1994)]. For Mab231, optimal superposition of V_L-V_H would require a relative rotation of 2.3°, marginally within that range.

In Figure 6 equivalent hypervariable loops maintain essentially the same course. Based on the work of Chothia *et al*. (1989) and other crystallographic studies [see review by Wilson and Stanfield (1994)], such similarities in backbone structure are to be expected (Table 4). Rigid body motions of loops arising from differences in crystallographic environment were not observed. For five of the six hypervariable loops, only slight side chain differences were noted (Figure 6), with H3 exhibiting the greatest due to movements of tyrosine residues 100H and 100I. CDR-H3 also demonstrated the greatest Cα rms deviation, 0.84 Å. While surfaces of hypervariable regions appear marginally different as a consequence of side chain movements, both exhibit a pronounced groove running through their antigen binding site. The binding sites are predominately hydrophobic, with only three charged residues, two Asp and one Lys, occurring in the hypervariable loop sequences (Table 4).

Hypervariable Loop Packing. Packing of molecules in the crystal involves extensive contacts which impose order on otherwise mobile elements. In particular, these include interactions of Fab hypervariable loops with Fc segments where switch peptides join C_H2 to C_H3. The Fab CDRs of each antibody interact with Fc segments of two neighboring molecules. Fab1 contacts Fc heavy chain 1 of one molecule, while Fab2 interacts with Fc heavy chain 2 of another. The interactions are similar, but not identical. As seen in Figure 7, the two Fabs associate with C_H2-C_H3 switch peptides, hypervariable loop H3 providing the principal contact in both cases. The buried surface area was 427 Å^2 for Fab1 and 498 Å^2 for Fab2 (Table 5), tempting speculation that these contacts could be similar to an antibody−antigen interaction. Indeed, CDRs H3 and L3 in contact with antigens appear to be favored in such instances [for review, see Sheriff (1993b) and Wilson and Stanfield (1994)].

An examination of Table 5 shows that the interaction between the hypervariable region of Fab1 and chain 1 C_H2:C_H3 involves nine antibody residues, of which seven are CDR amino acids and only two are framework residues. Association between Fab2 and chain 2 C_H2:C_H3 uses a total of 11 antibody amino acids; nine of these are CDR residues and only two from the framework. Buried surface area,

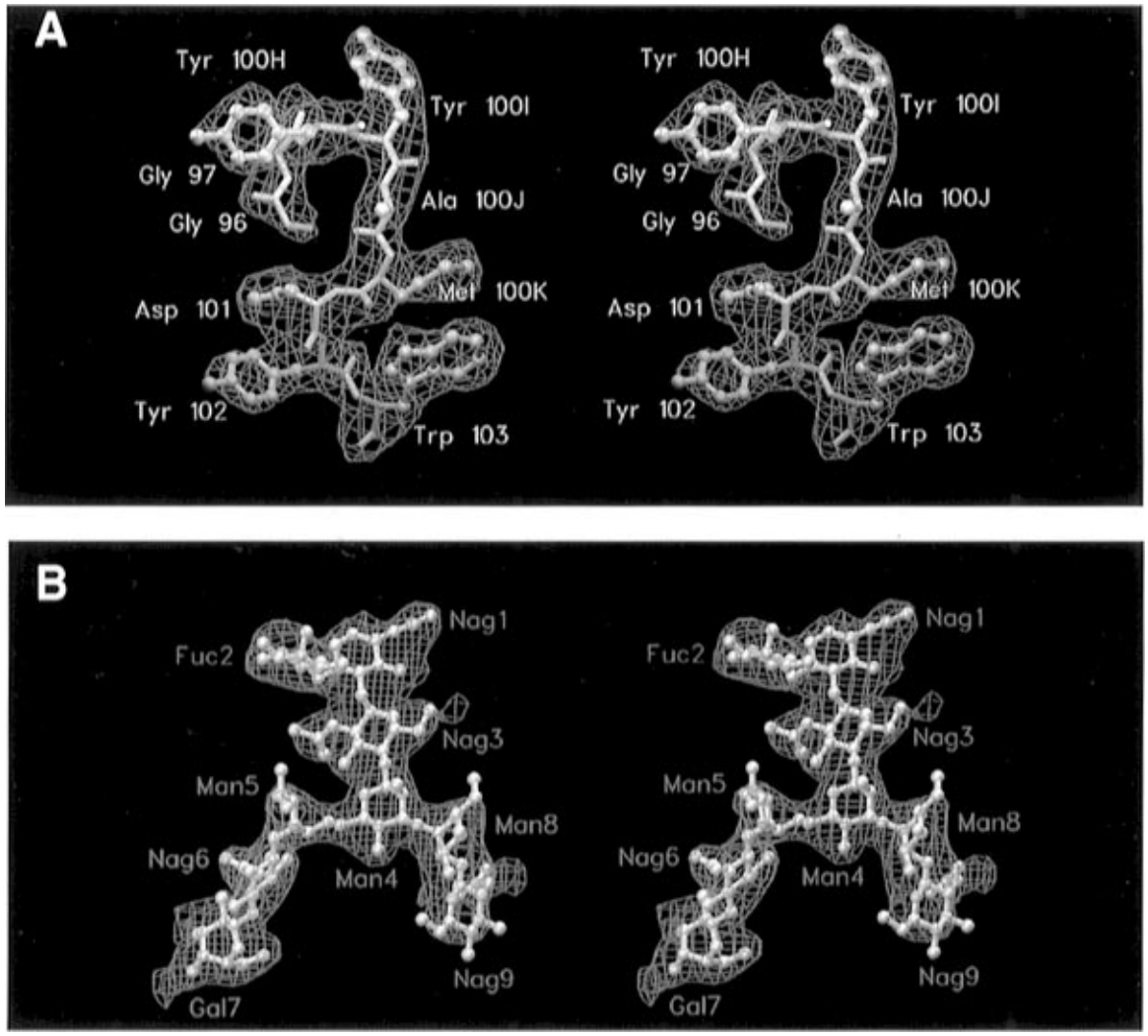

FIGURE 4: (A) Electron density of a Powell minimized $F_o - F_c$ omit map, contoured at 3.0 σ, with the corresponding structure of Fab2 hypervariable loop H3 and framework residues Tyr102 and Trp103. (B) Electron density of a Powell minimized $F_o - F_c$ omit map, contoured at 2.5σ, with the corresponding oligosaccharide structure from heavy chain 1 of the Fc segment. The carbohydrate N-links to Asn314 on the C_H2 domain.

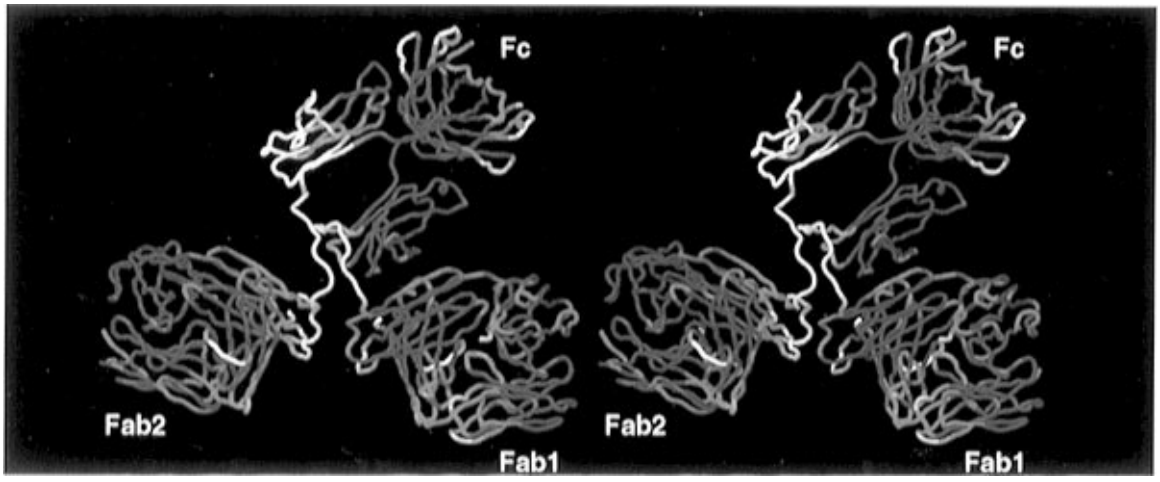

FIGURE 5: Canine lymphoma antibody backbone shown colored according to local temperature factors; dark blue designates low *B*-values, red higher, and white highest. Consistent with their appearance in electron density maps, the upper portions of one C_H2 domain and the hinge polypeptides clearly have a high degree of mobility. Some external loops of the structure also display high thermal factors.

hydrogen bonds, and other interactions are consistent with those found for other antibody−antigen complexes where the antigen was a peptide (Sheriff, 1993b).

The possibility that contacts, observed in the crystal between CDRs and switch peptides, reflect an antibody−antigen interaction is more plausible than it might first appear. The antigen for the antibody described here, Mab231, has recently been identified as a 29 kDa membrane protein that is expressed on the surfaces of canine lymphoma cells (personal communication). They are otherwise absent

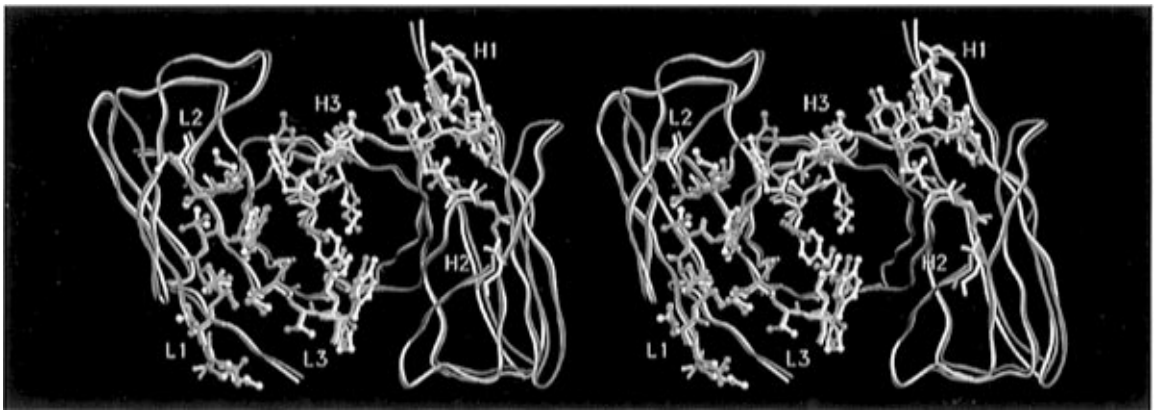

FIGURE 6: Stereo diagram of a Cα superposition of the variable domain pairs (V_L:V_H) of Fab1 and Fab2 as viewed directly into the antigen binding site. Fab1 is in white and Fab2 in blue-green. The rms deviation in Cα positions is 0.59 Å, using all Cα atoms for the calculation. The domain association of the variable pairs is near identical for the two Fabs; furthermore, equivalent CDRs maintain essentially the same course. Backbone and side chain atoms for the six CDRs are shown and labeled; L indicates light chain CDRs and H indicates heavy chain (see Table 4 for CDR amino acid sequences). Rigid body movements of the hypervariable loops were anticipated due to different chemical environments for the Fabs, but they were not observed. For five of the six hypervariable loops only slight side chain differences were noted. Hypervariable loop H3 exhibited the greatest side chain movement involving, particularly, Tyr100H and Tyr100I. Loop H3 also had the largest Cα rms deviation, 0.84 Å.

Table 4: Sequences and Conformations of V_L and V_H Hypervariable Regions[a]

	hypervariable loop sequence							framework residues				canonical structure
L1				*				*	*	*	*	
	26	27	28	29	30	31	32	2	25	33	71	
	Ser	Gln	Asn	Ile	Asn	Val	Trp	Ile	Ala	Leu	Phe	2
L2								*	*			
	50	51	52					48	64			
	Lys	Ala	Ser					Ile	Gly			1
L3					*			*				
	91	92	93	94	95	96		90				
	Gly	Gln	Ser	Tyr	Pro	Leu		Gln				1
H1	*	*		*				*	*			
	26	27	28	29	30	31	32	34	94			
	Gly	Phe	Thr	Phe	Ser	Asp	Tyr	Met	Arg			1
H2			*					*				
	52A	53	54	55				71				
	Asn	Gly	Gly	Gly				Arg				3
H3												
	96	97	100H	100I	100J	100K	101					
	Gly	Gly	Tyr	Tyr	Ala	Met	Asp					

[a] The canonical structure number refers to the conformations described by Chothia *et al*. (1989), and the residues that are mainly responsible for these conformations are indicated by an asterisk. H3 does not have canonical classifications. Numbering according to Kabat *et al*. (1991).

or in very low number on the surfaces of normal lymphocytes. Based on binding pattern similarities with other antibodies against canine lymphomas, and a number of other immunological properties, it appears that Mab231 may bind to immune receptors on the malignant lymphocyte surfaces (Steplewski *et al*., 1987). These receptors are themselves members of the immunoglobulin structural superfamily and generally contain domains similar to C_H2 and C_H3 of an IgG, and these are joined by switch peptides or a homologue.

Thus it is reasonable that either or both of the CDR-switch peptide interactions, illustrated in Figure 7, might be similar in greater or lesser respects to a true antibody−antigen complex. If this is indeed so, then it is interesting to note that the modes of interaction of the switch peptides with the two Fabs are somewhat different. It has, however, been previously observed that Fab binding sites can accommodate different orientations of an antigen with even nanomolar affinities (Arevalo *et al*., 1993, 1994).

It may also be relevant that the antibody studied here exhibits some "cryoglobulin-like" properties, in that it tends to precipitate at cold temperature under low salt conditions. Cryoglobulins are often identified with autoimmune diseases such as rheumatoid arthritis, and their self-association is frequently mediated by interactions of hypervariable regions with Fc segments of other molecules (Cruse & Lewis, 1995). The Kol immunoglobulin, for example, is a cryoglobulin (Marquart *et al*., 1980). Its crystal lattice is maintained by contacts involving hypervariable loops with hinge polypeptides, interactions suggested by the Kol investigators to possibly reflect those producing cryoprecipitate formation.

Hinge Region. The hinge sequence for the mouse IgG2a anti-canine lymphoma antibody, with residue numbering according to the convention of Kabat *et al*. (1991), is

```
      Upper        Core        Lower
226                                    250
  EPRGPTIKP  CPPCKCP  APNLLGG
  |--------genetic hinge-------|
           |---------structural hinge---------|
```

The three cysteine residues in the core (Cys237, Cys240, Cys242)form inter-heavy chain disulfide bonds. Cys128 of

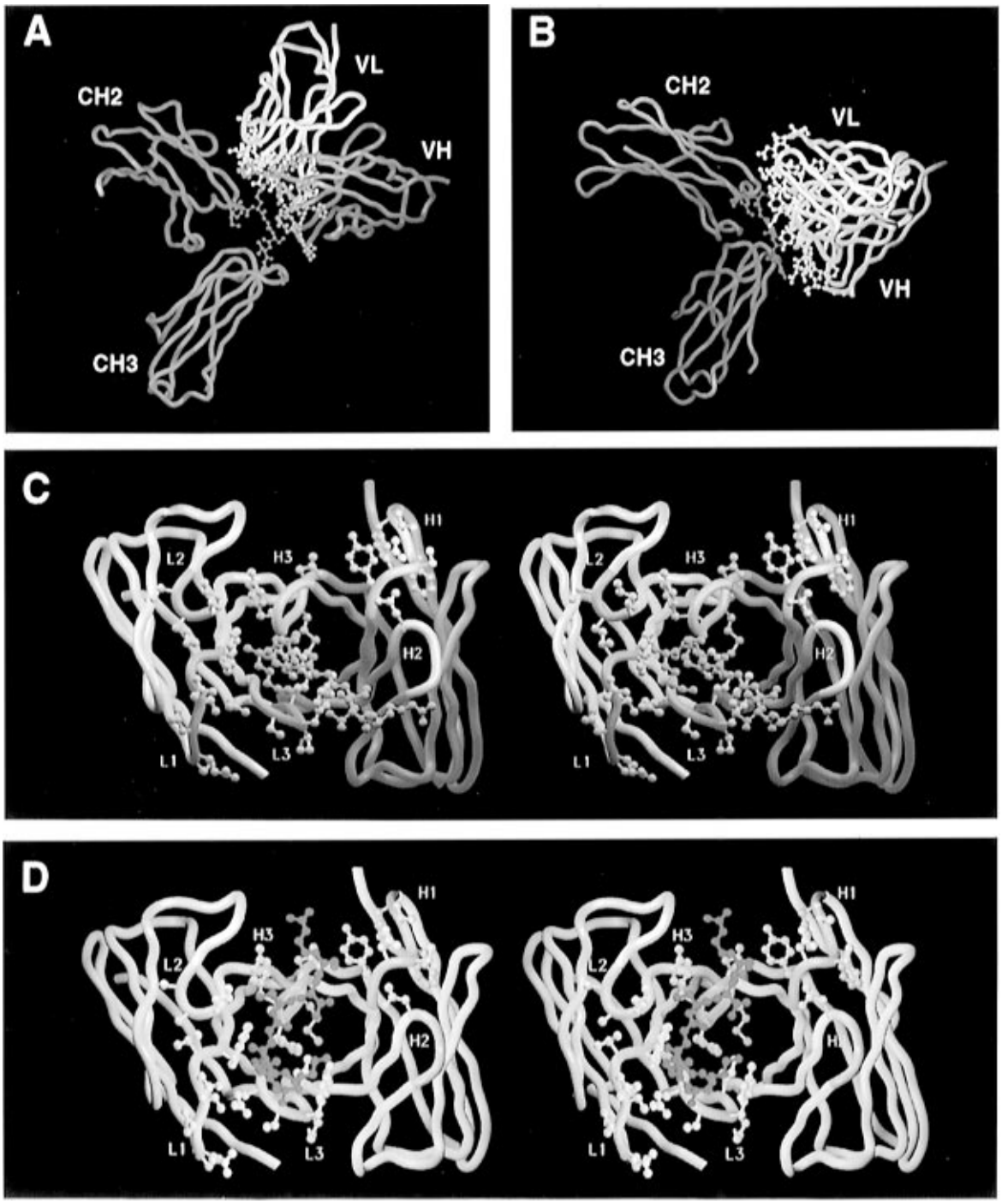

FIGURE 7: Representations of two primary intermolecular contacts responsible for formation and maintenance of the antibody crystal. These involve (A) the association of Fab1 hypervariable loops with the Fc C_H2-C_H3 switch peptide of heavy chain 1 of a second IgG molecule (0, −1, 1) and (B) a similar, though not identical, contact of Fab2 with heavy chain 2 of a third antibody (−1, 1, 0). In (C) and (D) these interactions are shown in detail. The C_H2-C_H3 switch peptides of heavy chain 1 (green) and that of heavy chain 2 (red) are bound by the CDRs of Fab1 and Fab2, respectively, using principally loop H3 in both cases. The extent of buried surface area and the presence of hydrogen bonds suggest that these interactions, seen here in the crystal, may occur as well under other conditions.

the C_H1 domain bonds with the terminal cysteine of the light chain (Cys214) to form the heavy−light chain disulfide.

Once the structure was near convergence, the hinge polypeptides emerged from difference Fourier maps. Electron density for the entire hinge, encompassing residues 226 through 250, became completely continuous at a contour level of 1σ, and much was visible at 2σ (Figure 8A). The upper hinge from Glu226 to Pro236 was clearly present at a 2σ contour level, including both main and side chain atoms. The first five upper hinge residues (Glu226 through Pro230), considered "structurally" to belong to the Fab, although a part of the "genetic hinge", closely maintain the dyad of the C_L:C_H1 domain pairs.

Temperature factors rise in a consistent manner from about 60 Å^2 at Arg228 to over 120 Å^2 at Thr231, indicative of the onset of mobility in the upper hinge. The "swivel region" includes Thr231 through Lys235. Though the electron density remains interpretable over this segment, the dyad relationship between the two heavy chains dissipates.

The hinge core, Cys237 through Pro243, includes three disulfides at Cys237, Cys240, and Cys242. The electron density corresponding to residues Cys237, Pro238, and

Table 5: Packing of Fab Hypervariable Loops with Symmetry-Related Fcs

(A) Interactions between Fab1 (0, 0, 0) and Fc Heavy Chain 1 (0, −1, 1)

	in contact				
segment	residues	atoms	H bonds	salt links	VDWs
Fab1 V_L:V_H total	9	29	3	2	40
Fab1−V_L	6	17	2	2	25
L-CDR1	3	12	2	0	19
L-CDR2	1	3	0	2	3
L-CDR3	1	1	0	0	2
Fab1−V_H	3	12	1	0	15
H-CDR1	0	0	0	0	0
H-CDR2	0	0	0	0	0
H-CDR3	2	10	0	0	13
Fc chain 1 total	7	19	3	2	40
Fc 1−C_H2	5	14	2	2	25
Fc 1−switch	2	5	1	0	15
Fc 1−C_H3	0	0	0	0	0

(B) Interactions between Fab2 (0, 0, 0) and Fc Heavy Chain 2 (−1, 1, 0)

	in contact				
segment	residues	atoms	H bonds	salt links	VDWs
Fab2 V_L:V_H total	11	27	2	0	49
Fab2−V_L	3	7	0	0	12
L-CDR1	1	5	0	0	9
L-CDR2	1	1	0	0	1
L-CDR3	1	1	0	0	2
Fab2−V_H	8	20	2	0	37
H-CDR1	1	4	0	0	4
H-CDR2	2	4	0	0	8
H-CDR3	3	10	2	0	23
Fc chain 2 total	9	24	2	0	49
Fc 2−C_H2	1	1	0	0	1
Fc 2−switch	4	16	2	0	34
Fc 2−C_H3	4	7	0	0	14

	buried		
segment	residues	atoms	surface area (Å^2)
Fab1 V_L:V_H total	24	66	427
Fab1−V_L	13	37	293
Fab1−V_H	11	29	134
Fc chain 1 total	20	61	405
Fc 1−C_H2	11	37	256
Fc 1−switch	5	16	123
Fc 1−C_H3	4	8	26

	buried		
segment	residues	atoms	surface area (Å^2)
Fab2 V_L:V_H total	26	74	498
Fab2−V_L	7	16	103
Fab2−V_H	19	58	395
Fc chain 2 total	23	65	512
Fc 2−C_H2	3	6	22
Fc 2− switch	7	26	249
Fc 2−C_H3	12	33	241

[a] Pairwise contacts were calculated using CONTACSYM (Sheriff, 1993b). Van der Waals interactions were to a maximum of 4.11 Å; hydrogen bonds were included up to a distance of 3.4 Å and salt links to 3.8 Å length. Buried surface areas were calculated using MS (Connolly, 1983) with a probe sphere of 1.6 Å. Complementary determining region (CDR) sequences used for the calculations are listed in Table 4. C_H2−C_H3 switch sequence = KPKGSVR (residues 358−365). Lys50 of Fab1 CDR L2 and Glu337 of C_H2 form the salt bridge. Glu337, Lys339, and Lys341 comprise the proposed complement C1q binding site on C_H2 (Duncan & Winter, 1988).

Pro239 (particularly Pro238) was consistently more ambiguous than any other part of the hinge core and was, in fact, only comparable to some parts of the weak lower hinge region. On the other hand, Cys240-Lys241-Cys242-Pro243 were well defined by electron density (Figure 8B), including the side chain of Lys241.

Residues Ala244 through Gly250 are genetically part of the C_H2 domain but structurally belong to the lower hinge. This segment is clearly the most mobile portion, and was the most difficult to interpret, of the entire hinge. The two heavy chains making up this region were not, however, equivalent, heavy chain 2 appearing better defined in electron density maps. We noted that this segment on heavy chain 2 followed a path which would allow it to contact and possibly hydrogen bond with the exposed loop, Asn344−Pro350, of its C_H2 domain. This was not the case for the corresponding segment on heavy chain 1.

In the lower hinge, side chain density was present but diffuse for residues Asn246, Leu247, and Leu248. These side chains were set to zero occupancy in the final model. In this model, of the 46 hinge residues, all main chain atoms were given full occupancy, while a total of six side chains were assigned zero occupancy.

Overall, the hinge, having an extent of 50 Å, is clearly very fluid and flexible, likely a continuum of conformations rather than a small, discrete set. This appears consistent with NMR studies of another IgG2a antibody (Kim *et al.*) and further suggests that the "hinge" is not, in fact, a structural hinge but a "tether" or link between Fc and Fabs. In this crystal, there are no packing interactions involving any part of the hinge. The relative dispositions of the Fc and Fab segments, however, undoubtedly reflect packing contacts, and therefore, the hinge structure seen here could be indirectly influenced by the packing of molecules in the lattice.

Fc Segment. The Fc structure presented here, as a component of the intact anti-lymphoma antibody, is the first example of a murine Fc determined by X-ray crystallography. It is 65% identical in amino acid sequence to the human Fc fragment solved previously, and there are no insertions or deletions. As might be anticipated, the remainder of the amino acid sequence is highly homologous; thus, the human and mouse Fc domain structures are, with the exceptions described below, virtually the same.

The C_H2 domains of the Mab231 Fc exhibit a pseudo-2-fold relationship of 177.8°. C_H3 domains also have a nearly exact dyad with a rotation angle of 178.8°. While domain pairs C_H2:C_H2 and C_H3:C_H3 are related by two different pseudo-2-fold axes, they are very close and yield, overall, a nearly exact 2-fold relationship for the entire Fc segment (Table 3).

In structures of intact myeloma IgG (Silverton *et al.*, 1977; Guddat *et al.*, 1993) and the human Fc/fragment B of protein A complex (Deisenhofer, 1981) heavy chains were related by crystallographic symmetry, but analysis of free human Fc fragment (Deisenhofer, 1981) and the human Fc/fragment C2 of protein G complex (Sauer-Eriksson *et al.*, 1995) revealed the symmetry to be only approximate. A comparison, illustrated in Figure 9, of the Fc segment of the canine lymphoma antibody with the free human Fc fragment, as well as with structures of Fc fragments complexed with either protein A or protein G, shows that the C_H3:C_H3 domains can be superimposed with a Cα rms deviation of about 1.0 Å. Distinctive differences in the Fc fragments exist,

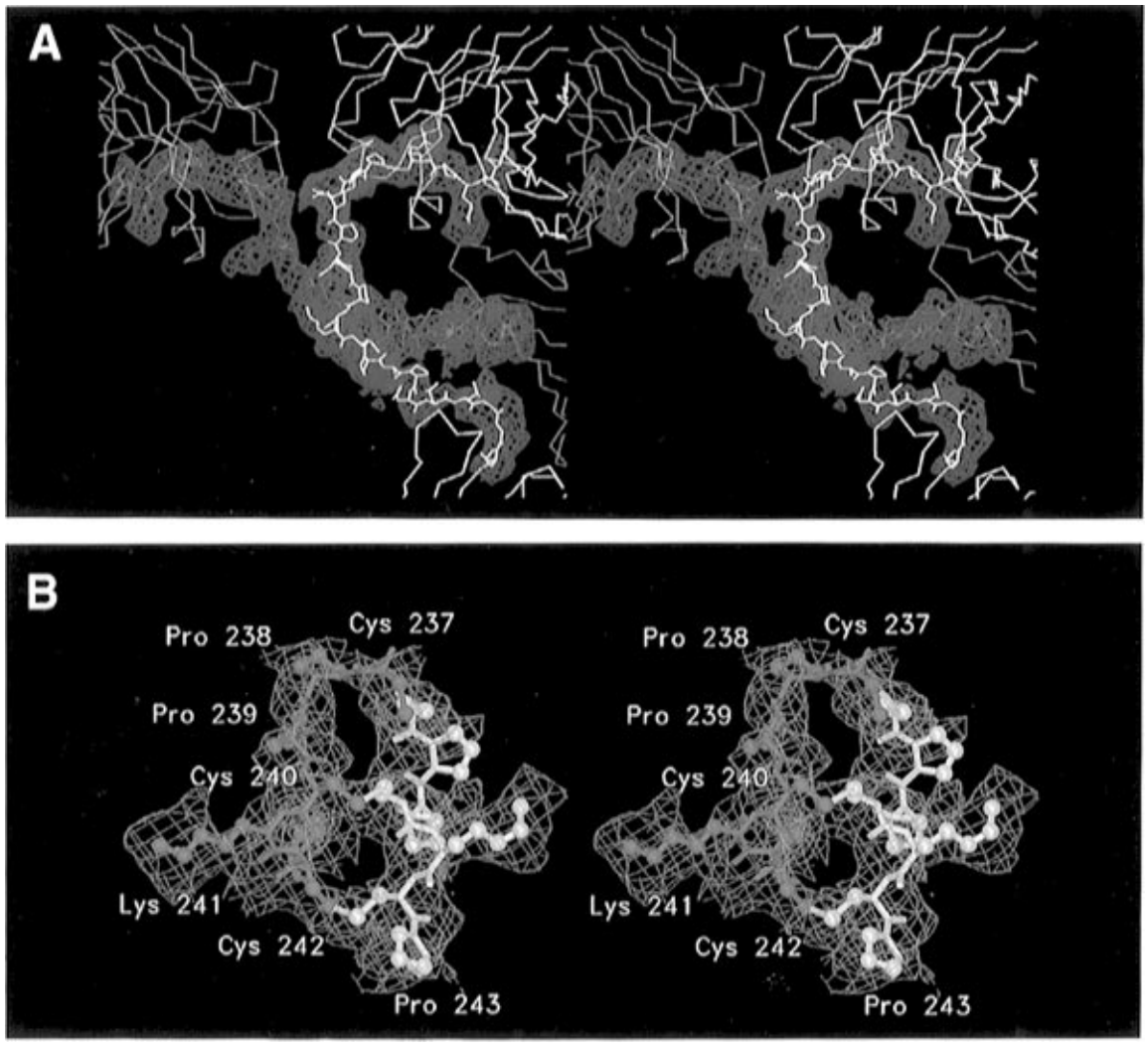

FIGURE 8: (A) Hinge polypeptides (residues 226−250) of both heavy chains shown with corresponding electron density of a Powell minimized $F_o - F_c$ omit map, contoured at 1 σ. Heavy chain 1 is in red and heavy chain 2 in white. Fab light chains are in orange. The hinge is composed of a rigid, though mobile core, flanked above and below by highly fluid regions. (B) Electron density of a Powell minimized $F_o - F_c$ omit map, contoured at 1.3 σ, for the hinge core with corresponding residues Cys237 through Pro243. The three inter-heavy chain disulfide bonds are indicated in yellow.

however, regarding the disposition of their C_H2 domains. C_H2 domains of the anti-lymphoma antibody can only be superimposed on those of the free human Fc, if they undergo rigid body rotations of 8.6° for heavy chain 1 C_H2 and 16.6° for chain 2 C_H2. In this intact murine antibody, the C_H2 domains have diverged from one another and inclined toward C_H3: C_H3 as compared to their dispositions in the other free and liganded Fcs (see Figure 9). It is somewhat curious that in the Mab231 IgG, which has an intact hinge with a core of disulfides linking its two C_H2 domains, these domains are spread further apart than in any of the other Fc or Fc−protein structures. This is in spite of the fact that all the other Fc structures were independent fragments lacking any hinge constraint.

Figure 9 illustrates an additional structural feature that may be of physiological relevance. For all of the Fc structures, in spite of rigid body motions, the helical loop comprised of residues Pro257−Pro270 remains almost invariant in its orientation and position with respect to the C_H3 domains. This loop forms the principal contact interface between the C_H2 and C_H3 domains and seems to serve as the "pivot" for the C_H2 rigid body motion. It may be relevant as well that this structurally invariant pivot is also a major element in the binding sites of a wide range of effector proteins (see discussion below).

Flexibility within the Fc would permit a greater diversity of conformations for the entire IgG molecule and could provide a mechanism for the modulation of effector functions. Based on analyses to date, however, movements of C_H2 domains with respect to C_H3 domains appear substantially more limited than for Fab elbow motions which aid in antigen recognition and binding.

Carbohydrate Component. Two biantennary, complex oligosaccharides, which fortuitously have the same sequence as that assigned to the human Fc (Deisenhofer, 1981), N-link through Asn314 (EU number 297) to the Fc C_H2 domains of Mab231. This was deduced from the carbohydrate composition for Mab231 in combination with sequence information for oligosaccharides of monoclonal antibodies produced by murine hybridomas (Rothman *et al*., 1989; Krotkiewski *et al*., 1990; Coco-Martin *et al*., 1992; Patel *et al*., 1992). It was immediately apparent from difference Fourier syntheses that the cores of the oligosaccharides occupied essentially the same locations as for the human Fc structure and, furthermore, they interacted with the same amino acid residues. The model carbohydrate of the human

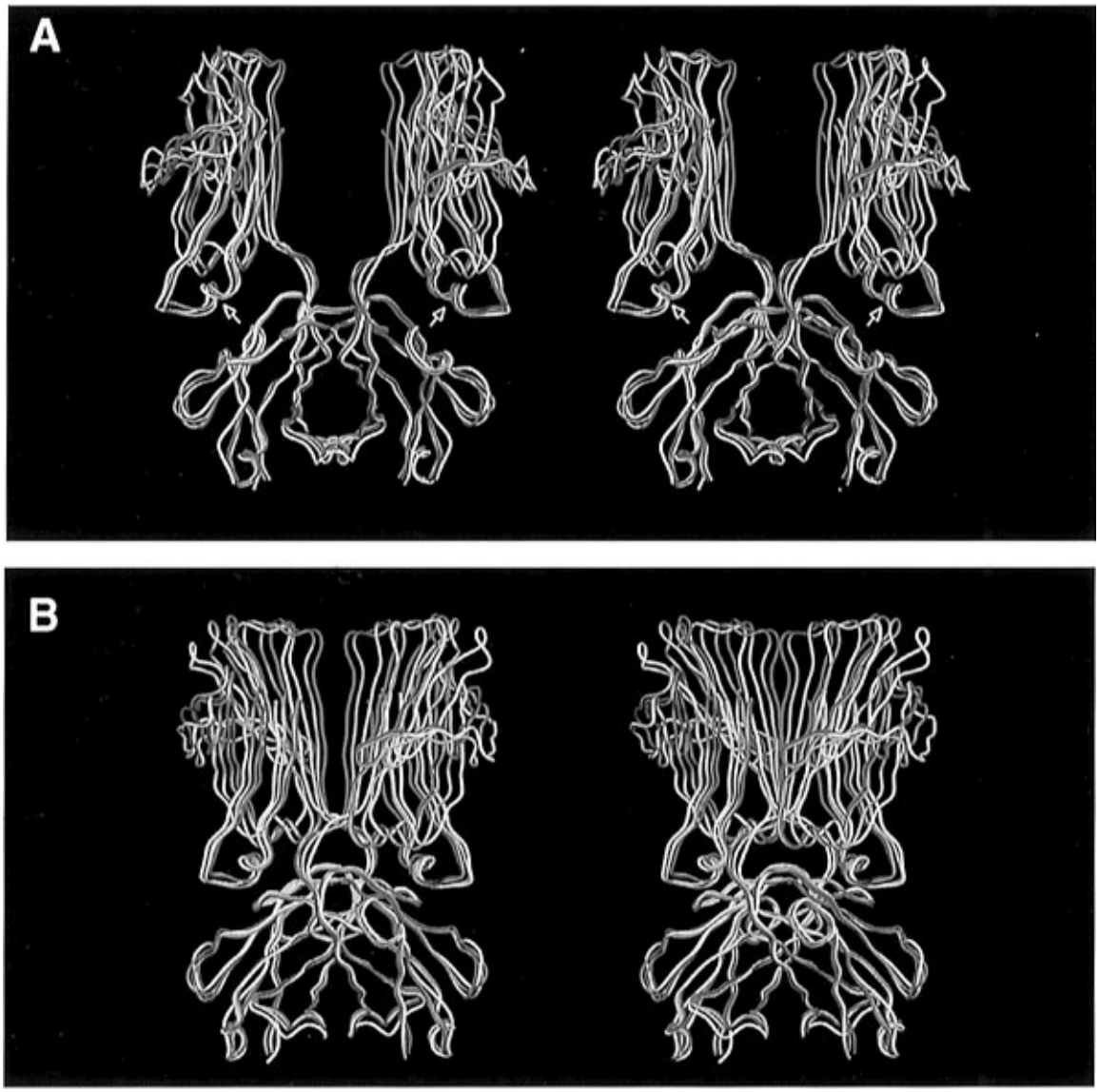

FIGURE 9: C_H3 domains of crystallographically determined Fc fragment structures, the free human Fc (blue) (Deisenhofer, 1981), the human Fc from its complex with protein A (red) (Deisenhofer, 1981), and the human Fc from its complex with protein G (yellow) (Sauer-Eriksson *et al*., 1995), optimally superimposed upon the C_H3 domain pair of the intact, murine Mab231 IgG (white). If the C_H3 domains are, as here, made congruent, the C_H2 domains display a range of rigid body rotations with respect to one another. (A) and (B) represent two views of this comparison of the polypeptide backbones. The free human Fc (initial molecular replacement model) and the Fc portion of the free intact IgG represent near extremes of the distribution, with the C_H2 domains of the intact antibody furthest apart and those of the free human Fc fragment closer together. Rotations of 8.6° and 16.6° are required to superimpose exactly the two C_H2 domains without altering the relative C_H3 dispositions. The hinge segment does not appear to impose any significant constraint on the relative orientations of the C_H2 domains. It may be relevant that the only part of the C_H2 domain that remains fixed, with respect to the C_H3 domains, is the helical loop (residues 257−270, indicated with arrows) that forms a major part of the C_H2-C_H3 interface. This loop seems to serve as the "pivot" for the C_H2 rigid body movement.

Fc fragment (chain A) required only slight adjustment to fit into $2F_o - F_c$ maps of Mab231.

The entire oligosaccharides on both Fc chains were visible; however, the sugars on heavy chain 1 were better ordered (Figure 4B). The carbohydrate components closely maintain the pseudo-dyad relationship between C_H2 domains (Figure 3), as seen also in the structure of the human Fc (Deisenhofer, 1981). No contact is made between Mab231 carbohydrate moieties of the two heavy chains, but sugar residues do interact with side chains of the protein. Some primary protein residues involved in sugar contacts are Phe254, Phe256, Lys259, Asp262, Thr273, and Tyr313. When the human Fc oligosaccharide is compared to the Mab231 carbohydrate, the principal differences lie in the orientation and placement of Fuc2 and of the branch ends Gal7 and Nag9 (Figure 10). The fucose residue may be of particular interest. In both this antibody and the human Fc it interacts with Tyr313, but the interactions are quite different in the two cases. This fucose is also near the Fcγ receptor binding site and could influence binding by the receptor.

A major difference between the human Fc and this murine Fc, involving the carbohydrate, is that no contacts of any form are made between the two oligosaccharides in the latter case. Inter-sugar chain contacts and hydrogen bonds exist within the human Fc fragment which result in what was described as a "weak bridge" (Deisenhofer, 1981). In the human Fc, this carbohydrate-mediated interaction provided the only contact between C_H2 domains; thus in the murine Fc seen here, there are no contacts at all between C_H2 domains. Nonetheless, in both the human and murine Fc, a

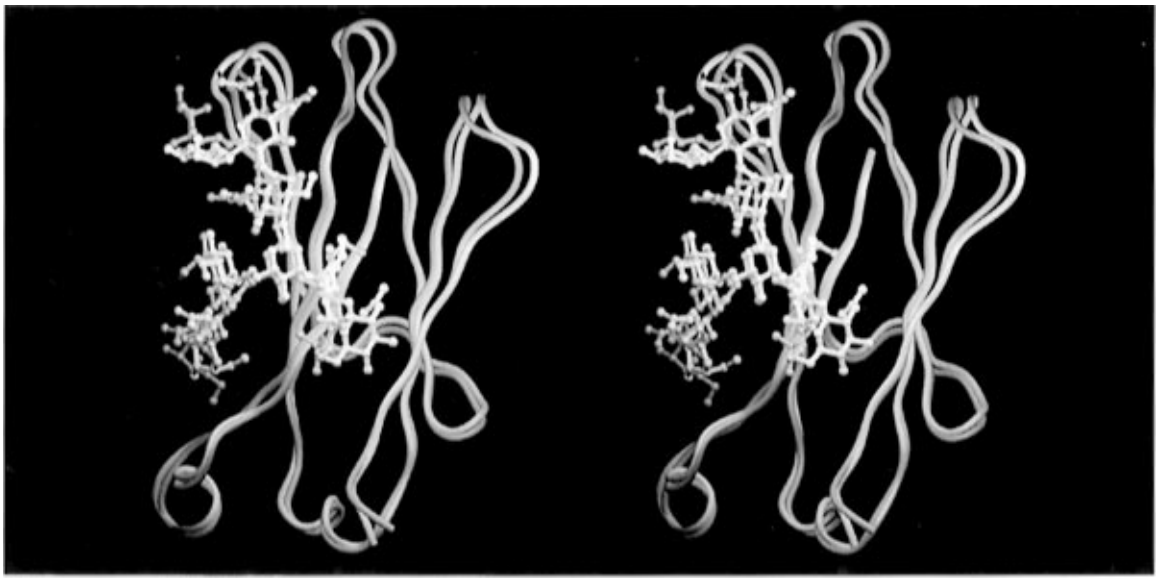

FIGURE 10: Comparison of the branched oligosaccharide moiety of the intact IgG (white) with the oligosaccharide of the free human Fc fragment (beige) described previously (Deisenhofer, 1981). The C_H2 backbones were optimally superimposed. As seen here, the cores of the two carbohydrate chains are virtually congruent, but variations in the orientations of terminal sugar residues exist. The greatest difference is in the disposition of the fucose residue branching from the first Nag.

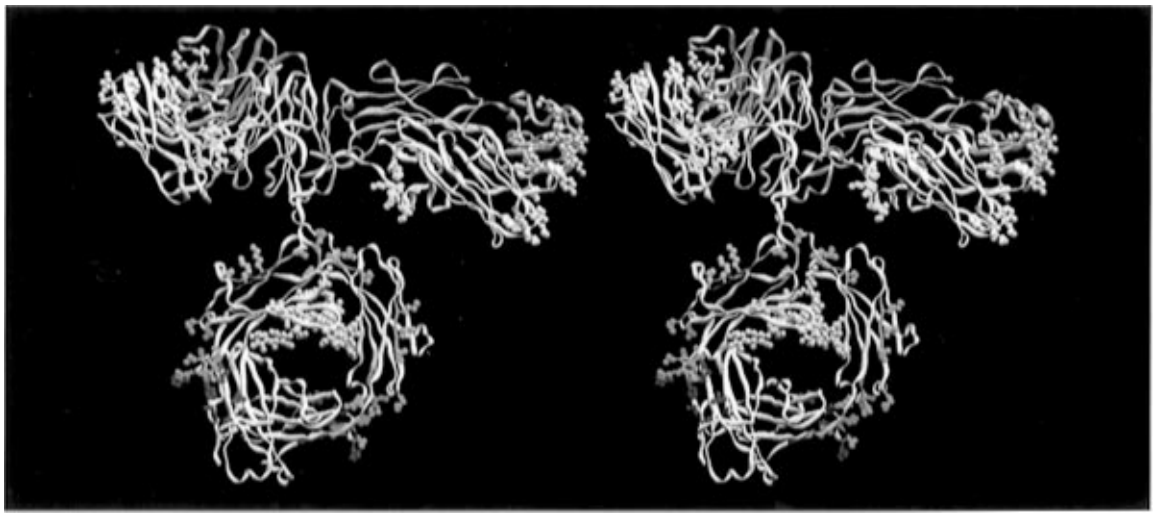

FIGURE 11: Side chains implicated in other studies as forming binding sites for various biologically important molecules color coded on a ribbon representation of the intact IgG for canine lymphoma. Antibody light chains are in pale blue, while heavy chains are in white. Fab2 is in front and Fab1 in back. Oligosaccharides are represented by gray CPK. Hypervariable loops involved in antigen recognition are emphasized in two shades of lavender. Core binding sites for effector function molecules, complement protein C1q and Fcγ receptors (FcRI, FcRII, and FcRIII), are colored in orange and cyan, respectively. It is likely, however, that multiple contact points will occur when large effector molecules such as these dock with intact IgG. Bacterial Fc receptors bind at the Fc C_H2-C_H3 interface: protein A and protein G common contact points are indicated in green; unique protein A contacts are shown in red and protein G in dark purple. The rat neonatal Fc receptor (FcRn) and rheumatoid factor also bind a site overlapping where proteins A and G contact. A second, independent site for protein G binding is indicated on the Fab C_H1 domains in yellow.

dyad relationship between C_H2 domains exists. This relationship must, therefore, arise from constraints imposed by the interface with the C_H3 domains.

Effector Functions. Figure 11 is a representation of the anti-lymphoma antibody showing elements of the structure having particular interest or unique biological function. Residues comprising the heavy and light chain hypervariable loops, which make up the antigen binding sites, are emphasized at the extreme ends of the Fab arms. The distance between the H3 loops of the two Fabs is 151 Å (measured from equivalent Tyr100H Cαs). Binding of antigens on the tumor cell surface separated by greater distances would require spreading apart of the Fabs, a motion restricted ultimately by the core of disulfides in the hinge. The distance between H3 loops and the farthest point on C_H3:C_H3 of the Fc (chain2 Glu450) is about 130 Å for Fab1 and 120 Å for Fab2, but this could vary substantially depending on the disposition assumed by the Fc with respect to the Fab segments. The closest distance from any part of an Fab to the Fc is about 15 Å, specifically from Fab2's C_H1 domain to C_H2 of heavy chain 1.

The carbohydrate components linked to the heavy chains at Asn314 can be seen occluding the cavity at the center of the Fc. No direct evidence, that we know of, suggests that the oligosaccharides form part of any effector binding site. Degradation or modification of the carbohydrate has, however, been clearly shown to eliminate or reduce effector functions such as complement activation, binding to Fc

receptors, induction of antigen-dependent cellular cytotoxicity, and feedback immunosuppression [reviewed in Furukawa and Kobata (1991)]. Galactose residues, in particular, have been demonstrated to be of significant importance for immunological function (Tsuchiya *et al*., 1989). Indeed, there is evidence from H-NMR that conformational changes in the sugar chains can affect the structure of the Fc (Matsuda *et al*., 1990).

Bacterial proteins A and G bind at the region of the C_H2-C_H3 junction in the Fc segment (Deisenhofer, 1981; Sauer-Eriksson *et al*., 1995). In Figure 11, amino acid side chains uniquely bound by proteins A and G are shown in red and dark purple, respectively, while residues bound in common (264−267, 330, and 465) are in green. It may be significant that residues 264−267 comprise the first loop of C_H2, a loop that is noticeably consistent in its orientation (see above) with respect to the C_H3 domains in every case where an Fc has been visualized (see also Figure 9).

Interfaces between C_H2 and C_H3 domains are clearly of significance in terms of association with other immunologically important molecules. For example, the region bound by proteins A and G has also been defined crystallographically as the overlapping binding site for rat neonatal Fc receptor (FcRn) (Burmeister *et al*., 1994) as well as for rheumatoid factor (Corper *et al*., 1996). Biochemical studies, in addition, have indicated this area as the regulatory site for both catabolism and transcytosis control [for review, see Ghetie and Ward (1995)].

Residues 119, 121, and 215−222, shown in yellow in the C_H1 domains of the Fab segments, are secondary binding sites for protein G (Derrick & Wigley, 1992). Protein A also has a secondary binding site on the Fab, specifically on molecules expressing V_HIII isotype (Sasso *et al*., 1989). A third bacterial Ig receptor, protein L, binds to the variable domain of κ light chain (Akerström & Björck, 1989), yet the exact contact residues on the antibody have not been defined. Ig-binding proteins, such as protein A, G, or L, have been suggested to be important for bacterial virulence (Kastern *et al*., 1990; Raeder & Boyle, 1993).

Amino acids 247−251, highlighted in cyan, are involved in the association with high-affinity Fcγ receptor, FcRI, which is found predominantly on human monocytes (Duncan *et al*., 1988). These FcRI recognition residues make up part of the lower hinge region. The other two classes of human leukocyte Fcγ receptors, FcRII and FcRIII, have additionally been shown to interact with sites which are distinct but overlap that for FcRI (Lund *et al*., 1991; Sarmay *et al*., 1992; Morgan *et al*., 1995). An electrostatic analysis of the surrounding area, near these Fc receptor contact sites at the lower hinge, was performed with the program GRASP (Nicholls *et al*., 1991). The three upper loops of the C_H2 domain (residues 278−286, 313−318, and 344−350) were found to form an acidic surface or platform which could, because of close proximity, be involved in the complex docking interaction.

The anti-lymphoma antibody presented here does activate complement (Rosales *et al*., 1988). The residues shown to be involved in direct binding by the hydra heads of C1q (Glu337, Lys339, and Lys341) are found on the rather mobile C_H2 domains (Duncan & Winter, 1988) and are designated in orange. All IgG isotypes contain this "core" C1q-binding motif; thus, this site alone cannot account for observed differences in complement activation by the antibody subclasses [see review by Brekke *et al*., (1995)]. The centers of these clusters of amino acids are 70 Å and 88 Å from the nearest H3 loop, which is that of Fab2, and are 113 and 103 Å from H3 of Fab1.

The question remains as to how binding of antigen could promote complement activation since Fc and Fab segments are spatially decoupled. The picture of the antibody provided here seems to lend further support to ideas dependent on the association or aggregation of Fc segments from neighboring, antigen-anchored IgG molecules to trigger these activities. Indeed, the flexibility and mobility implied by this structure are entirely consistent with a model relying on "dislocation" of Fcs from the plane of the Fabs and formation of clusters from spatially allied units [for review, see Burton (1990) and Burton and Woof (1992)]. The core hinge, Cys237−Pro243, would in that case provide a kind of stem, while upper hinge residues, Thr231−Lys235, and lower hinge residues, Ala244−Gly250, would serve as swivels.

The various binding sites for effector proteins and their physiological significance have been thoroughly reviewed elsewhere and will not be discussed further here (Burton & Woof, 1992). As has been previously noted, virtually all of the effector functions are distributed over the surface of the Fc segment and appear independent of Fab influence. This is consistent with the high degree of internal mobility suggested by this model.

Conclusions. Individual Fab and Fc segments of the Mab231 antibody, the constituent constant and variable domains of the Fabs, as well as C_H2 and C_H3 domains of the Fc, have notably different relative dispositions from those observed in other X-ray crystallographic studies of intact IgG (Silverton *et al*., 1977; Guddat *et al*., 1993; Marquart *et al*., 1980). The structure illustrates the independence of Fab and Fc segments (Figure 3), features suggested by other analyses using a variety of methods (Wrigley *et al.*, 1983; Roux, 1984; Wade *et al.*, 1989; Schneider *et al.*, 1988; Dangl *et al.*, 1988; Huber *et al.*, 1976; Amzel & Poljak, 1979). The conformation observed in this analysis is likely to be but one of many, but one which has been selected by the constraints of lattice interactions. In solution, intact IgG molecules presumably occupy a variety of structural states, ranging from distorted T-shapes to distorted Y-shapes, as a consequence of inherent domain mobility. This antibody is best described as a distorted T-shape.

The first five upper hinge residues maintain the Fabs' constant domain 2-fold; otherwise, no well-defined relationship exists between the heavy chain segments comprising the hinge region (Figure 8). These polypeptides serve as linkers and probably assume whatever conformation is necessary to maintain the Fabs and Fc joined. The conformation of the hinge polypeptide, which is not really a hinge at all, but a "tether", is ultimately determined by the dispositions of the antigen binding Fabs and the effector activating Fc. There is no indication from this structure of any contrary influence.

The observation that hypervariable regions of both Fab segments have nearly identical conformations in different crystallographic environments (Figure 6) suggests their plasticity may be limited; that is, their structures are relatively rigid and specified by their amino acid sequence. On the other hand, the hypervariable regions are, in a sense, "complexed" in that they make intimate and qualitatively

similar contacts with Fc switch peptides (Figure 7 and Table 5). This could provide an alternate explanation for the near identity of the CDRs and variable domain pair associations. If these crystal packing contacts are considered a "complex" interaction, then the minor differences in backbone and side chain atoms between corresponding CDRs of the two Fabs could be attributed to induced fit complementarity. Difference in elbow angles of the two Fabs could be a consequence of variable domain pairs adjusting to allow optimization of CDR contacts at the C_H2-C_H3 switch peptides.

Mab231 provides the first structure of a mouse Fc segment, all previous examples being of human or other origin [see review by Padlan (1994)]. A comparison of our mouse antibody Fc segment with free and complexed human Fc fragments (Deisenhofer, 1981; Sauer-Eriksson *et al*., 1995) revealed significant differences of C_H2 domain dispositions with respect to the C_H3 domain pair. The C_H2 domains of Mab231 diverge from one another compared to the corresponding human Fc domains and incline toward $C_H3:C_H3$, with switch peptides ensuring flexibility (Figure 9).

The altered spatial relationships of domains within the mouse Fc with respect to the human Fc appear significant, but it is unclear whether the observed differences are due to species variations or, more likely, are consequences of other structural considerations. The human Fcs were, for example, in every case fragments dissociated from the remainder of the antibody. The Fc in Mab231, on the other hand, may sense structural influences or constraints imposed by continuity with the hinge and, ultimately, with the Fabs. The observed conformation could, furthermore, reflect the interactions of hypervariable regions from neighboring Fabs with switch peptides, though this seems to us less likely.

Certainly the most remarkable feature exemplified by the Mab231 antibody structure is the intrinsic segmental flexibility of the molecule. This undoubtedly reflects the functional requirements placed on the IgG. Following antigen binding by CDRs of the Fab segments, Fc-dependent associations apparently occur to trigger effector functions such as activation of complement or stimulation of immune system cells, i.e., macrophages. Thus, stable and highly stereospecific binding at three independent sites must be coincidentally maintained. In addition, each of the three sites of binding may be in motion with respect to others. Such binding would be difficult, perhaps impossible to achieve, except by a flexible "adapter" molecule like that seen here (Figure 11).

ACKNOWLEDGMENT

We thank the San Diego Supercomputer Facility for time granted on the Cray C-90, the Stanford Synchrotron Radiation Laboratory (SSRL) for time granted to collect diffraction data, and the Graphics and Visual Imaging Lab at UCR for assistance with figures. We also extend thanks to Hartmut Luecke for help in data collection and processing at SSRL and to Aaron Greenwood for help with image production.

REFERENCES

Amzel, L. M., & Poljak, R. J. (1979) Three-dimensional structure of immunoglobulins, *Annu. Rev. Biochem. 48*, 961−997.

Akerström, B., & Björck, L. (1989) Protein L: an immunoglobulin light chain binding protein. Characterization of binding and physiological properties, *J. Biol. Chem. 264*, 19740−19746.

Alzari, P. M., Lascombe, M.-B., & Poljak, R. J. (1988) Three-dimensional structure of antibodies, *Annu. Rev. Immunol. 6*, 555−580.

Arevalo, J. H., Taussig, M. J., & Wilson, I. A. (1993) Molecular basis of cross-reactivity and the limits of antibody-antigen complementarity, *Nature 365*, 859−863.

Arevalo, J. H., Hassig, C. A., Stura, E. A., Sims, M. J., Taussig, M. J., & Wilson, I.A. (1994) Structural analysis of antibody specificity. Detailed comparison of five Fab′-steroid complexes, *J. Mol. Biol. 241*, 663−690.

Ban, N., Escobar, C., Hasel, K. W., Day, J., Greenwood, A., & McPherson, A. (1995) Structure of an anti-idiotypic Fab against feline peritonitis virus-neutralizing antibody and a comparison with the complexed Fab, *FASEB J. 9*, 107−114.

Bernstein, F. C., Koetzle, T. F., William, G. J. B., Meyer, E. F., Brice, M. D., Rodgers, J. R., Kennard, O., Shimanonchi, T., & Tasumi, M. (1977) The protein databank: a computer-based archival file for macromolecular structures, *J. Mol. Biol. 112*, 535−542.

Brekke, O. H., Michaelsen, T. E., & Sandlie, I. (1995) The structural requirements for complement activation by IgG: does it hinge on the hinge?, *Immunol. Today 16*, 85−90.

Brünger, A. T. (1991) Simulated annealing in crystallography, *Annu. Rev. Phys. Chem. 42*, 197−223.

Burmeister, W. P., Huber, A. H., & Bjorkman, P. J. (1994) Crystal structure of the complex of rat neonatal Fc receptor with Fc, *Nature 372*, 379−383.

Burton, D. R. (1990) Antibody: the flexible adapter molecule, *Trends Biochem. Sci. 15*, 64−69.

Burton, D. R., & Woof, J. M. (1992) Human antibody effector function, *Adv. Immunol. 51*, 1−84.

Chothia, C., Lesk, A. M., Tramontano, A., Levitt, M., Smith-Gill, S. J., Air, G., Sheriff, S., Padlan, E. A., Davies, D., Tulip, W. R., Colman, P. M., Spinelli, S., Alzari, P. M., & Poljak, R. J. (1989) Conformations of immunoglobulin hypervariable regions, *Nature 342*, 877−883.

Coco-Martin, J. M., Brunink, F., van der Velden-de Groot, T. A. M., & Beuvery, E. C. (1992) Analysis of glycoforms present in two mouse IgG2a monoclonal antibody preparations, *J. Immunol. Methods 155*, 241−248.

Colman, P. M. (1988) Structure of antibody-antigen complexes: implications for immune recognition, *Adv. Immunol. 43*, 99−132.

Connolly, M. L. (1983) Analytical molecular surface calculation, *J. Appl. Crystallogr. 16*, 548−558.

Corper, A. L., Sohi, M. K., Jefferis, R., Steinitz, M., Feinstein, A., Beale, D., Taussig, M. J., & Sutton, B. J. (1996) Structure of a human IgM rheumatoid factor complexed with its autoantigen IgG Fc, *International Union of Crystallography XVII Congress and General Assembly*, Seattle, WA, Aug 8−17.

Crowther, R. A. (1972) The fast rotation function, In *The Molecular Replacement Method* (Rossman, M. G., Ed.) pp 173−178, Gordon & Breach, New York.

Cruse, J. M., & Lewis, R. E. (1995) *Illustrated Dictionary of Immunology*, pp 197−198, 263, CRC Press, Boca Raton, FL.

Dangl, J. L., Wensel, T. G., Morrison, S. L., Stryer, L., Herzenberg, L. A., & Oi, V. T. (1988) Segmental flexibility and complement fixation of genetically engineered chimeric human, rabbit and mouse antibodies, *EMBO J. 7*, 1989−1994.

Davies, D. R., & Chacko, S. (1993) Antibody structure, *Acc. Chem. Res. 26*, 421−427.

Davies, D. R., Padlan, E. A., & Sheriff, S. (1990) Antibody-antigen complexes, *Annu. Rev. Biochem. 59*, 439−473.

Deisenhofer, J. (1981) Crystallographic refinement and atomic models of a human Fc fragment and its complex with fragment B of protein A from *Staphylococcus aureus* at 2.9- and 2.8-Å resolution, *Biochemistry 20*, 2361−2370.

Derrick, J. P., & Wigley, D. B. (1992) Crystal structure of a streptococcal protein G domain bound to an Fab fragment, *Nature 359*, 752−754.

Duncan, A. R. & Winter, G. (1988) The binding site for C1q on IgG, *Nature 332*, 738−740.

Duncan, A. R., Woof, J. M., Partridge, L. J., Burton, D. R., & Winter, G. (1988) Localization of the binding site for the human high-affinity Fc receptor on IgG, *Nature 332*, 563−564.

Edmundson, A. B., Wood, M. K., Schiffer, M., Hardman, K. D., Ainsworth, C. F., Ely, K. R., & Deutsch, H. F. (1970) A crystallographic investigation of a human IgG immunoglobulin, *J. Biol. Chem. 245*, 2763−2764.

Edmundson, A. B, Guddat, L. W., & Anderson, K. N. (1993) Crystal structures of intact IgG antibodies, *ImmunoMethods 3*, 197−210.

Edmundson, A. B., Guddat, L. W., Shan, L., & Fan, Z.-C. (1994) Structural aspects of conformational changes in ligand binding by antibody fragments, *Res. Immunol. 145*, 56−61.

Ely, K. R., Colman, P. M., Abola, E. E., Hess, A. C., Peabody, D. S., Parr, D. M., Connell, G. E., Laschinger, C. A., & Edmundson, A. B. (1978) Mobile Fc region in the Zie IgG2 cryoglobulin: comparison of crystals of the F(ab′)$_2$ fragment and the intact immunoglobulin, *Biochemistry 17*, 820−823.

Evans, S. V. (1993) SETOR: Hardware lighted three-dimensional solid model representations of macromolecules, *J. Mol. Graphics 11*, 134−138.

Fitzgerald, P. M. D. (1988) MERLOT, an integrated package of computer programs for the determination of crystal structures by molecular replacement. *Appl. Crystallogr. 21*, 273−276.

Furukawa, K., & Kobata, A. (1991) IgG galactosylation-its biological significance and pathology, *Mol. Immunol. 28*, 1333−1340.

Ghetie, V., & Ward, E. S. (1995) Genetic manipulation of antibodies: from variable domains to constant regions, in *The Antibodies* (Zanetti, M., & Capra, J. D., Eds.) pp 169−211, Harwood Academic, Australia and United States.

Guddat, L. W., Herron, J. N., & Edmundson, A. B. (1993) Three-dimensional structure of a human immunoglobulin with a hinge deletion, *Proc. Natl. Acad. Sci. U.S.A. 90*, 4271−4275.

Guddat, L. W., Shan, L., Anchin, J. M., Linthicum, D. S., & Edmundson, A. B. (1994) Local and transmitted conformational changes on complexation of an anti-sweetener Fab, *J. Mol. Biol. 263*, 247−274.

Hamlin, R., Cork, C., Howard, A., Nielsen, C., Vernon, W., Mathews, D., & Xuong, N.-H. (1981) Characteristics of a flat multiwire area detector for protein crystallography, *J. Appl. Crystallogr. 14*, 85−89.

Harris, L. J., Larson, S. B., Hasel, K. W., Day, J., Greenwood, A., & McPherson, A. (1992) The three-dimensional structure of an intact monoclonal antibody for canine lymphoma, *Nature 360*, 369−372.

Harris, L. J., Skaletsky, E., & McPherson, A. (1995) Crystallization of intact monoclonal antibodies, *Proteins 23*, 285−289.

Huber, R., Deisenhofer, J., Colman, P. M., & Matsushima, M. (1976) Crystallographic structure studies of an IgG molecule and an Fc fragment, *Nature 264*, 415−420.

Jeglum, K. A. (1989) Chemotherapy of Canine Lymphoma, *Proceedings of the Seventh ACVIM Forum*, San Diego, CA, pp 922−925.

Jones, T. A. (1978) A graphics model building and refinement system for macromolecules, *J. Appl. Crystallogr. 11*, 268−272.

Jones, T. A., & Kjeldgaard, M. (1994) *O-The Manual*, Uppsala University Press, Uppsala.

Kabat, E. A., Wu, T. T., Perry, H. M., Gottesman, K. S., & Foeller, C. (1991) in *Sequences of Proteins of Immunological Interest*, 5th ed., U.S. Public Health Service, NIH, Washington, DC.

Kastern, W., Holst, E., Nielsen, E., Sjöbring, U., & Björck, L. (1990) Protein L, a bacterial immunoglobulin-binding protein is a possible virulence factor, *Infect. Immun. 58*, 1217−1222.

Kim, H., Matsunaga, C., Yoshino, A., Kato, K., & Arata, Y. (1994) Dynamical structure of the hinge region of immunoglobulin G as studied by ^{13}C nuclear magnetic resonance spectroscopy, *J. Mol. Biol. 236*, 300−309.

Kleywegt, G. J., & Jones, T. A. (1995) Where freedom is given, liberties are taken, *Structure 3*, 535−540.

Kleywegt, G. J., & Jones, T. A. (1996) Good model-building and refinement practice, *Methods Enzymol.* (in press).

Krotkiewski, H., Grönberg, G., Krotkiewska, B., Nilsson, B., & Svensson, S. (1990) The carbohydrate structures of a mouse monoclonal IgG antibody OKT3, *J. Biol. Chem. 254*, 20195−20201.

Larson, S., Day, J., Greenwood, A., Skaletsky, E., & McPherson, A. (1991) Characterization of crystals of an intact monoclonal antibody for canine lymphoma, *J. Mol. Biol. 222*, 17−19.

Lascombe, M.-B., Alzari, P. M., Boulot, G., Saludjian, P., Tougard, P., Berek, C., Haba, S., Rosen, E. M., Nisonoff, A., & Poljak, R. J. (1989) Three dimensional structure of Fab R19.9, a monoclonal murine antibody specific for the P-azobenzenearsonate group, *Proc. Natl. Acad. Sci. U.S.A. 86*, 607−611.

Laskowski, R. A., MacArthur, M. W., Moss, D. S., & Thornton, J. M. (1993) Procheck-a program to check the stereochemical quality of protein structures, *J. Appl. Crystallogr. 26*, 283−291.

Leslie, A. G. W. (1992) Recent changes to the MOSFLM package for processing film and image plate data, *Joint CCP4 and ESF-EACBM Newsletters on Protein Crystallography*, Vol. 26.

Lund, J., Winter, G., Jones, P. T., Pound, J. D., Tanaka, T., Walker, M. R., Artymiuk, P. J., Arata, Y., Burton, D. R., Jefferis, R., & Woof, J. M. (1991) Human FcγRI and FcγRII interact with distinct but overlapping sites on human IgG, *J. Immunol. 147*, 2657−2662.

Marquart, M., Deisenhofer, J., Huber, R., & Palm, W. (1980) Crystallographic refinement and atomic models of the intact immunoglobulin molecule Kol and its antigen-binding fragment at 3.0 Å and 1.9 Å resolution, *J. Mol. Biol. 141*, 369−391.

Matsuda, H., Nakamura, S., Ichikawa, Y., Kozai, K., Takano, R., Nose, M., Endo, S., Nishimura, Y., & Arata, Y. (1990) Proton nuclear magnetic resonance studies of the structure of the Fc fragment of human immunoglobulin G1: comparisons of native and recombinant proteins, *Mol. Immunol. 27*, 571−579.

Mian, I. S., Bradwell, A. R., & Olson, A. J. (1991) Structure, function and properties of antibody binding sites, *J. Mol. Biol. 217*, 133−151.

Morgan, A., Jones, N. D., Nesbitt, A. M., Chaplin, L., Bodmer, M. W., & Emtage, J. S. (1995) The N-terminal end of the C_H2 domain of chimeric human IgG1 anti-HLA-DR is necessary for C1q, FcγRI and FcγRIII binding, *Immunology 86*, 319−324.

Nicholls, A., Sharp, K., & Honig, B. (1991) Protein folding and association-insights from the interfacial and thermodynamic properties of hydrocarbons, *Proteins: Struct., Funct., Genet. 4*, 281−296.

Padlan, E. A. (1994) Anatomy of the antibody molecule, *Mol. Immunol. 31*, 169−217.

Padlan, E. A., Silverton, E. W., Sheriff, S., Cohen, G. H., Smith-Gill, S. J., & Davies, D. R. (1989) Structure of an antibody-antigen complex: crystal structure of the HyHEL-10 Fab-lysozyme complex, *Proc. Natl. Acad. Sci. U.S.A. 86*, 5938−5942.

Palm, W., & Colman, P. M. (1974) Preliminary X-ray data from well-ordered crystals of a human immunoglobulin G molecule, *J. Mol. Biol. 82*, 587−588.

Patel, T. P., Parekh, R. B., Moellering, B. J., & Prior, C. P. (1992) Different culture methods lead to differences in glycosylation of a murine IgG monoclonal antibody, *Biochem. J. 285*, 839−845.

Poljak, R. J., Amzel, L. M., Chen, B. L., Phizackerley, R. P., & Saul, F. (1974) The three dimensional structure of the Fab fragment of a human myeloma immunoglobulin at 2.0 angström resolution, *Proc. Natl. Acad. Sci. U.S.A. 71*, 3440−3444.

Raeder, R., & Boyle, M. D. P. (1993) Association of type II immunoglobulin G-binding protein expression and survival of group A streptococci in human blood, *Infect. Immun. 61*, 3696−3702.

Rosales, C., Jeglum, K. A., Obrocka, M., & Steplewski, Z. (1988) Cytolytic activity of murine anti-dog lymphoma monoclonal antibodies with canine effector cells and complement, *Cell Immunol. 115*, 420−428.

Rothman, R. J., Warren, L., Vliegenthart, J. F. G., & Härd, K. J. (1989) Clonal analysis of the glycosylation of immunoglobulin G secreted by murine hybridomas. *Biochemistry 28*, 1377−1384.

Roux, K. H. (1984) Direct demonstration of multiple VH allotopes on rabbit Ig molecules: allotope characteristics and Fab arm rotational flexibility revealed by immunoelectron microscopy, *Eur. J. Immunol. 14*, 459−464.

Sarmay, G., Lund, J., Rozsnayay, Z., Gergely, J., & Jefferis, R. (1992) Mapping and comparison of the interaction sites on the Fc region of IgG responsible for triggering antibody dependent cellular cytotoxicity (ADCC) through different types of human Fc receptors, *Mol. Immunol. 29*, 633.

Sasso, E., Silverman, G., & Mannik, M. (1989) Human IgA and IgG F(ab′)$_2$ that bind to staphylococcal protein A belong to the V_HIII subgroup, *J. Immunol. 142*, 2778−2783.

Satow, Y., Cohen, G. H., Padlan, E. A., & Davies, D. R. (1986) Phosphocholine binding immunoglobulin Fab McPC603, *J. Mol. Biol. 190*, 593−604.

Sauer-Eriksson, A. E., Kleywegt, G. J., Uhlen, M., & Jones, T. A. (1995) Crystal structure of the C2 fragment of streptococcal protein G in complex with the Fc domain of human IgG, *Structure 3*, 265−278.

Schneider, W. P., Wensel, T. G., Stryer, L., & Oi, V. T. (1988) Genetically engineered immunoglobulins reveal structural features controlling segmental flexibility, *Proc. Natl. Acad. Sci. U.S.A. 85*, 2509−2513.

Sheriff, S. (1993a) Antibody-protein complexes, *ImmunoMethods 3*, 222−227.

Sheriff, S. (1993b) Some methods for examining the interactions between two molecules, *ImmunoMethods 3*, 191−196.

Sheriff, S., Silverton, E. W., Padlan, E. A., Cohen, G. H., Smith-Gill, S. J., Finzel, B. C., & Davies, D. R. (1987) Three-dimensional structure of an antibody-antigen complex, *Proc. Natl. Acad. Sci. U.S.A. 84*, 8075−8079.

Silverton, E. W., Navia, M. A., & Davies, D. R. (1977) Three-dimensional structure of an intact human immunoglobulin, *Proc. Natl. Acad. Sci. U.S.A. 74*, 5140−5144.

Stanfield, R. L., Takimoto-Kamimura, Rini, J. M., Profy, A. T., & Wilson, I. A. (1993) Major antigen-induced domain rearrangements in an antibody, *Structure 1*, 83−93.

Steplewski, Z., Jeglum, K. A., Rosales, C., & Weintraub, N. (1987) Canine lymphoma-associated antigens defined by murine monoclonal antibodies, *Cancer Immunol. Immunother. 24*, 197−201.

Stura, E. A., Satterthwait, A. C., Calvo, J. C., Stefanko, R. S., Langeveld, J. P., & Kaslow, D. C. (1994) Crystallization of an intact monoclonal antibody (4B7) against *Plasmodium falciparum* malaria with peptides from the Pfs25 protein antigen, *Acta Crystallogr. D50*, 556−562.

Suh, S. W., Bhat, T. N., Navia, M. A., Cohen, G. H., Rao, D. N., Rudikoff, S., & Davies, D. R. (1986) The galactan-binding immunoglobulin Fab J539: an X-ray diffraction study at 2.6 Å resolution, *Proteins 1*, 74−80.

Terry, W. D., Matthews, B. W., & Davies, D. R. (1968) Crystallographic studies of a human immunoglobulin, *Nature 220*, 239−241.

Tsuchiya, N., Endo, T., Matsuta, K., Yoshinoya, S., Aikawa, T., Kosuge, E., Takeuchi, F., Miyamoto, T., & Kobata, A. (1989) Effects of galactose depletion from oligosaccharide chains on immunological activities of human IgG, *J. Rheumatol. 16*, 285−290.

Wade, R. H., Taveau, J. C., & Lamy, J. N. (1989) Concerning the axial rotational flexibility of the Fab regions of immunoglobulin G, *J. Mol. Biol. 206*, 349−356.

Wilson, I. A., & Stanfield, R. L. (1994) Antibody-antigen interactions: new structures and new conformational changes, *Curr. Opin. Stuct. Biol. 4*, 857−867.

Wilson, I. A., Rini, J. M., Fremont, D. H., Fieser, G. G., & Stura, E. A. (1991) X-ray crystallographic analyses of free and antigen-complexed Fab fragments to investigate structural basis of immune recognition, *Methods Enzymol. 203*, 153−176.

Wrigley, N. G., Brown, E. B., & Skehel, J. J. (1983) Electron microscopic evidence for the axial rotation and inter-domain flexibility of the Fab regions of immunoglobulin G, *J. Mol. Biol. 169*, 771−774.

Xuong, N.-H., Nielsen, C., Hamlin, R., & Anderson, D. (1985) Strategy for data collection from protein crystals using a multiwire counter detector diffractometer, *J. Appl. Crystallogr. 18*, 342−360.

BI962514+